uOttawa

L'Université canadienne
Canada's university

FACULTÉ DES ÉTUDES SUPÉRIEURES ET POSTOCTORALES

uOttawa

L'Université canadienne
Canada's university

FACULTY OF GRADUATE AND POSDOCTORAL STUDIES

Yannick Gratton
AUTEUR DE LA THÈSE / AUTHOR OF THESIS

M.Sc. (Physics)
GRADE / DEGREE

Department of Physics
FACULTÉ, ÉCOLE, DÉPARTEMENT / FACULTY, SCHOOL, DEPARTMENT

Tethered Polymers in a Shear Flow:
A Molecular Dynamics study of the good and bad solvent cases

TITRE DE LA THÈSE / TITLE OF THESIS

Gary Slater
DIRECTEUR (DIRECTRICE) DE LA THÈSE / THESIS SUPERVISOR

CO-DIRECTEUR (CO-DIRECTRICE) DE LA THÈSE / THESIS CO-SUPERVISOR

EXAMINATEURS (EXAMINATRICES) DE LA THÈSE / THESIS EXAMINERS

R. Hodgson

R. Munger

Gary W. Slater
LE DOYEN DE LA FACULTÉ DES ÉTUDES SUPÉRIEURES ET POSTDOCTORALES /
DEAN OF THE FACULTY OF GRADUATE AND POSTDOCORAL STUDIES

Tethered Polymers in a Shear Flow:

A Molecular Dynamics study of the good and bad solvent cases

by

Yannick Gratton

A thesis presented to the University of Ottawa
in fulfilment of the thesis requirement for the degree of
Master of Science in Physics

Ottawa, Ontario
June 27, 2005

Your file Votre référence
ISBN: 0-494-11283-2
Our file Notre référence
ISBN: 0-494-11283-2

Abstract

Nanotechnology is now a reality although it is still very much in its infancy. This being said much work still needs to be done. During the last past few decades, new experimental tools such as videomicroscopy and optical tweezers, which allow us to both visualize and manipulate in real time the dynamics of macromolecules, have emerged. These two tools alone provide endless possibilities. For example, it is now possible to tether a polymer at one end with optical tweezers while a constant flow of solvent extends it. If the chain is fluorescently labeled, dynamical properties can be extracted via videomicroscopy. In this thesis, we study a similar problem. With the help of Molecular Dynamics (MD) simulations, we examine the physics of a Freely Jointed Chain (FJC) tethered by one end to a hard surface while being submitted to a Poiseuille flow. A good solvent is used during the first part of this thesis, while for the second part, we look at the dynamics of the chain in poor solvents. In both cases, we compare actual stretching theories to our simulation data and extract the effects of Hydrodynamic Interactions (HI). For good solvents, we propose a new empirical equation which relates the unstretched fraction of the chain to the full range of shear rates. We also observe a peculiar cyclic motion of the chain which was first reported experimentally. For poor solvents, we study the collapsed chain properties while changing the strength of the shear flow linearly in time. A novel hysteretic effect for the chain extension as a function of shear rate is observed in our simulations.

Sommaire

La nanotechnologie est maintenant réalité même si elle n'en est qu'à ses débuts; beaucoup de travail reste encore à faire. Durant les dernières décennies, plusieurs nouveaux outils expérimentaux ont vu le jour, comme la vidéomicroscopie et les pinces optiques, qui, mis ensemble, permettent de visualiser et de manipuler des macromolécules individuelles en temps réel. Ces deux outils à eux seuls ouvrent la porte à d'innombrables possibilités. Par exemple, il est maintenant possible de tenir un polymère par un bout avec une pince optique, tout cela pendant qu'un courant de solvant l'étire. Si la chaîne est fluorescente, ses propriétés dynamiques peuvent être extraites via la vidéomicroscopie. Dans cette thèse, nous étudions un problème de ce type. Avec l'aide de simulations de dynamique moléculaire, nous examinons la physique d'une "Freely Jointed Chain" (FJC) attachée par un bout à une surface dure et soumises à un flux de type Poiseuille. Un bon solvant est utilisé pour la première partie de la thèse, alors que pour la deuxième partie, nous examinons les propriétés dynamiques d'une chaîne plongée dans un mauvais solvant. Dans les deux cas, nous comparons les théories actuelles d'étirement à nos résultats de simulation et nous en extrayons les effets des interactions hydrodynamiques. Pour de bons solvants, nous proposons une nouvelle équation empirique qui relie la fraction non-étirée d'une chaîne à la totalité des taux de cisaillement. De plus, nous observons un mouvement cyclique particulier de la chaîne, mouvement aussi observé expérimentalement. Pour de mauvais solvants, nous étudions les propriétés de chaînes effondrées sur elles-mêmes pendant que la force du courant de cisaillement varie en temps de façon linéaire. Un nouvel effet d'hystérésis, pour l'extention des chaînes en fonction du ratio de cisaillement, est observé lors de nos simulations.

Remerciements

Je veux remercier tout spécialement mon superviseur, l'infatiguable Gary, pour son temps employé à me diriger dans ma thèse lors de ces dernières années, pour son éternel enthousiasme ainsi que pour ses nombreux encouragements. Je veux remercier aussi Martin Kenward et Frédéric Tessier pour leur nombreuses heures passées à répondre à mes innombrables questions. De plus, comment pourrais-je ne pas mentionner l'atmosphère géniale présente dans le groupe de Gary incluant:

- Eric
- Frédéric
- Jean-François
- Katerina
- Laurette
- MartinB
- MartinK
- Michel
- Sébastien
- Simona
- Smaine
- Sorin
- Tatek

Cette thèse n'aurait pas pu voir le jour sans l'appui moral de ma fiancée Fanny ainsi que de ma famille au cours de mes études. Je tiens aussi à remercier le Fonds Nature et Technologies (Québec) ainsi que l'Université d'Ottawa pour les bourses allouées.

List of publications included in this thesis

This is a thesis by articles. It is based on work reported in the following two manuscripts:

I. Y. Gratton and G. W. Slater

Molecular Dynamics Study of Tethered Polymers in Shear Flow.

Accepted for publication in the European Physical Journal E (June 13, 2005).

II. Y. Gratton and G. W. Slater

Molecular Dynamics Study of Collapsed Tethered Polymers in Shear Flow.

To be submitted to European Physical Journal E.

Contents

Introduction

The limits of science and its associated technologies are being continually pushed forward by human perseverance and ingenuity. Many branches of science have started a rapid advance toward miniaturization, and new effects which have no macroscopic analogue are emerging at a phenomenal rate. This is analagous to the big push made during the last few decades towards reducing the size of components in the field of information technologies (e.g., semiconductors, computers, cell phones, etc.). In fact, the direction taken in this branch of science is called nanotechnology. Research is progressing in multiple sub-fields like nano-mechanical devices, quantum computers, biochips and nanochannels. For example, the use of nanofluidic channel technologies opens the door to the development of tools like ultra-fast lab-on-a-chip technologies [1]. It is possible to separate DNA molecules with ratchet systems [2], control flow profiles in microfluidic devices with polymer brushes tethered to the walls of a tube [3], lubricate capillary walls [4], etc. Other techniques like fluorescence microscopy enable us to see in real time the conformations of fluorescently-labelled polymers or DNA chains [5]. It has been found that the presence of polymer chains, diffusing freely in the channel or tethered to the channel walls [6], can influence dramatically the response of nanofluidic systems.

As is well known, a complex problem is often more easily understood by dividing it into small pieces (reductionism): once the foundation of knowledge is put into place, it may be easier to address the complexity of the original problem. The goal for this thesis is to solidify one of the theoretical building blocks in micro- and nano-channel science: the dynamics of a polymer chain tethered to a wall in a shear flow.

This thesis consists of two submitted manuscripts which examine, using Molecular Dynamics (MD) simulations, the dynamics of single tethered polymers in a shear flow. The thesis provides answers to the two following questions: Does the Ladoux and Doyle [7] polymer-deformation theory still hold for Freely Jointed Chains (FJC) when hydrodynamic interactions are present? Do we observe cyclic polymer motion in the presence of bad solvents? The first manuscript [I] addresses this problem from the point of view of a good solvent while the second manuscript [II] looks at the same problem in the presence of a poor solvent.

This Introduction is organized as follows. Section 1.1 describes the relevant basic concepts of polymer physics. Section 1.2 describes past studies or related work, both experimental and theoretical. Following this preamble and a discussion of our simulation method (Section 1.3), the two manuscripts

which constitute the main section of this thesis are discussed in Section 1.4. My other contributions (Section 1.5) as well as a statement of originality in Section 1.6 conclude the Introduction.

1.1 Polymer theory

From a scientific perspective there are many ways to envisage a polymer. For example, a mathematician sees it as a self-avoiding random walk. For a chemist, it is a long molecule with (usually) covalent bonds. The engineer sees it as a material with unlimited possibilities while the economist considers it one of the most profitable materials of the 20th century. Of course one physicist point of view is the one adopted in this thesis: a polymer is a thermodynamic object with many internal degrees of freedom. The word itself, "poly-mer", means "many units". As an example, Figure 1.1 shows a polyethylene chain which fits perfectly the description of the word "polymer". Polyethylene (perhaps one of the simplest polymers) is composed of identical repeating CH_2 groups that we call "monomers". Many different architectures of polymer molecules exist such as branched chains, cross-linked polymers and linear chains. In this thesis we focus our study on linear chains.

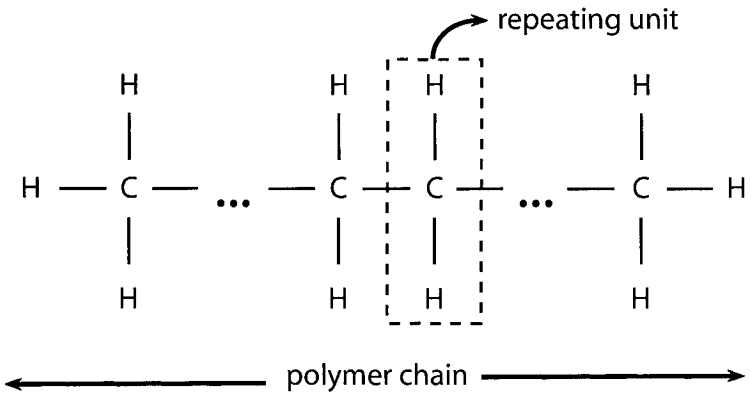

Figure 1.1: *Example of a polymer: the linear polyethylene molecule* $CH_3 - [CH_2]_n - CH_3$.

The ideal chain

As mentioned above, a chemist would look at a polymer at the level of the atom, but as physicists some of us prefer a more unified point of view and simplify the problem by modeling the polymer chain in a simpler representation. Let's consider an ideal chain composed of $n + 1$ backbone "atoms" A_i (with $0 \leq i \leq n$) where no net interaction exists between atoms that are not nearest neighbors along

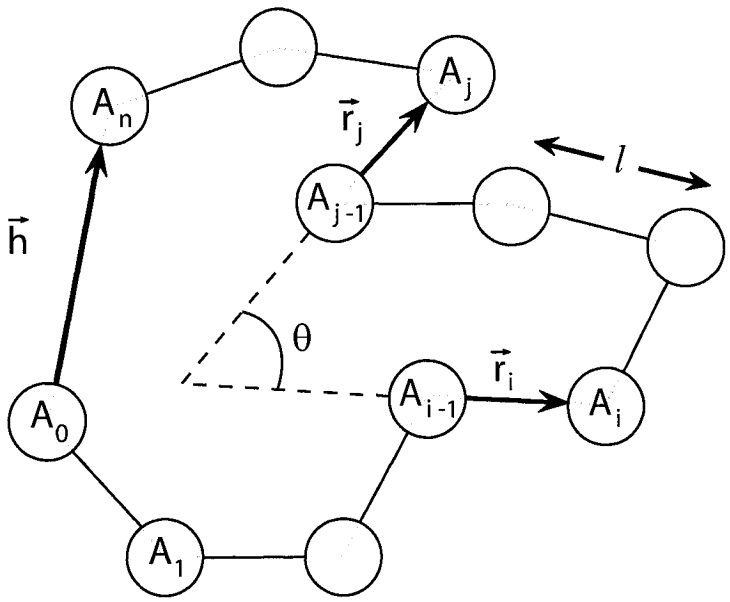

Figure 1.2: *The ideal chain model.*

the backbone of the chain (see Fig. 1.2). The bond vector $\vec{r}_i$ goes from atom A_{i-1} to atom A_i. The end-to-end vector $\vec{h}$ is defined as the sum of all bond vectors in the chain,

$$\vec{h} = \sum_{i=1}^{n} \vec{r}_i. \tag{1.1}$$

Since the mean end-to-end vector $\langle \vec{h} \rangle$ is zero due to the symmetry of rotation (note that the mean $\langle ... \rangle$ is over all possible conformations), the mean square end-to-end distance $\langle \vec{h}^2 \rangle$ becomes a useful average chain dimension for this problem. It is given by

$$\langle h^2 \rangle \equiv \langle \vec{h} \cdot \vec{h} \rangle = \sum_{i=1}^{n} \sum_{j=1}^{n} \langle \vec{r}_i \cdot \vec{r}_j \rangle. \tag{1.2}$$

For a fixed bond length l, the dot product between $\vec{r}_i$ and $\vec{r}_j$ as shown in Figure 1.2 corresponds to

$$\vec{r}_i \cdot \vec{r}_j = l^2 \cos\theta_{ij}. \tag{1.3}$$

If we assume that there is no direction correlations between bond vectors (i.e., $\langle \cos\theta_{ij} \rangle = 0$ for $i \neq j$ and $\cos\theta_{ij} = 1$ for $i = j$), and that we have a fixed bond length l, the resulting model is called the Freely Jointed Chain (FJC) model [8]. For a FJC, the mean square end-to-end distance becomes simply

$$\langle h^2 \rangle = nl^2 = h_{\max} l, \tag{1.4}$$

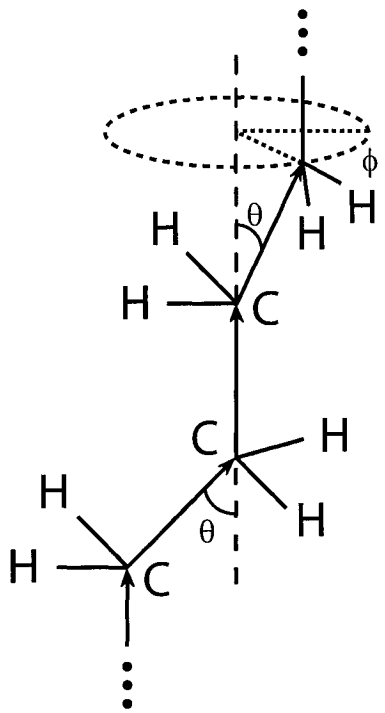

Figure 1.3: *The Freely Rotating Chain (FRC) model.*

where $h_{\max} = nl$ is the maximum end-to-end distance of the FJC.

In reality, correlations are usually present between neighboring bond vectors, which means that $\langle \cos\theta_{ij} \rangle \neq 0$. In this case we can use a variant of the FJC called the Freely Rotating Chain (FRC) model [9] which fixes the bond angles θ to a specific value while allowing the torsion angles ϕ to be randomly distributed between $-\pi$ and π (see Fig. 1.3). The mean square end-to-end distance for a FRC [8] can be approximated by

$$\langle h^2 \rangle = nl^2 \frac{1 + \cos\theta}{1 - \cos\theta}. \tag{1.5}$$

The fraction $\frac{1+\cos\theta}{1-\cos\theta}$ is called the Flory characteristic ratio C_∞. To recover the statistical properties of a FJC while taking into account the specificities of the FRC, one needs to redefine the number of effective monomers (N) and the effective length (b) of the freely jointed bonds. To illustrate the change of length scale from l to b, lets take for example a polyethylene molecule [8]. If we model a polyethylene chain as a FRC (see Fig. 1.4), its maximum end-to-end distance $h_{\max}$ in an all-trans conformation will be

$$h_{\max} = nl \cos\frac{\theta}{2} \equiv Nb. \tag{1.6}$$

Since $\langle h^2 \rangle$ must be equal in both models, for the same conditions we get

$$\langle h^2 \rangle = nl^2 C_\infty = Nb^2, \tag{1.7}$$

which gives the following relation for b (also called the Kuhn length):

$$b = \frac{nl^2 C_\infty}{nl \cos\frac{\theta}{2}} = \frac{lC_\infty}{\cos\frac{\theta}{2}}. \tag{1.8}$$

The number of bonds N then becomes

$$N = \frac{\left(nl\cos\frac{\theta}{2}\right)^2}{nl^2 C_\infty} = \frac{n\left(\cos\frac{\theta}{2}\right)^2}{C_\infty}. \tag{1.9}$$

We have to point out that the new definitions of b and N (Eqs. (1.8) and (1.9)) give a FJC that has the same statistical properties as the FRC, but only for very long polymer chains (i.e., $h_{\max} \gg b$).

Since the bond angle $\theta = 68\,^\circ$ and the bond length $l = 0.154$nm for the polyethylene molecule, the Kuhn length $b \cong 0.41$nm.

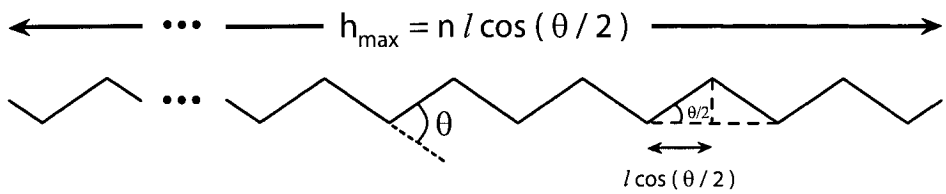

Figure 1.4: *An all-trans representation of the backbone of a polyethylene molecule.*

Worm-like chains

For shorter chains ($N \not\gg 1$), the relation $\langle h^2 \rangle = Nb^2$ is inadequate. The chain is not long enough to curve completely unto itself due to the angular constraints. If $\theta \to 0$ the chain looks like a worm which slowly curves along its backbone. A model was derived to explain the statistics behind this special case: the Worm-Like Chain (WLC) model [8–10]. A detailed calculation yields

$$\langle h^2 \rangle = b \times \left[h_{\max} + \frac{b}{2}\left(e^{-2h_{\max}/b} - 1\right)\right] \cong \begin{cases} h_{\max}^2 & N \not\gg 1 \\ bh_{\max} & N \gg 1. \end{cases} \tag{1.10}$$

A good example of a WLC is a double-stranded DNA molecule which has a Kuhn length $b \cong 100$ nm which is much larger than the natural base pair spacing of around 0.34 nm. We will not discuss further the properties of the WLC model since the core of this thesis is aimed at the FJC model.

Radius of gyration R_g

Another statistical property of a macromolecule is its radius of gyration R_g [9]. It is defined as the standard-deviation of the distribution of mass around the center of mass $\vec{R}_{cm}$ of the molecule

$$R_g^2 \equiv \frac{1}{N}\sum_{i=1}^{N}\langle\left(\vec{R}_i - \vec{R}_{cm}\right)^2\rangle \tag{1.11}$$

where $\vec{R}_i$ is the position of monomer i and $\vec{R}_{cm} = \frac{1}{N}\sum_{i=1}^{N}\vec{R}_i$. If we assume a FJC, the calculation gives

$$R_g^2 = \frac{1}{6}Nb^2 = \frac{\langle h^2\rangle}{6} \sim N. \tag{1.12}$$

Distribution function p(h)

The distribution function $p(h)$ is defined as the number of conformations $\Omega(h)$ with the same end-to-end distance $h \equiv |\vec{h}|$ divided by the total number of conformations, Ω_T. The FJC conformations can be represented by random walks. The simplest random walk is a one-dimensional (1D) problem. The probability of making a step in either direction is equal to 1/2. Also, for N steps, n_+ steps are taken to the right while $n_- = N - n_+$ are taken to the left, giving $h_x = n_+ - n_- = 2n_+ - N$. The probability of having an unbiased walk with a final distance of h_x along x is

$$p(h_x) = \Omega(h_x) \times \frac{1}{\Omega_T} = \frac{N!}{n_+!n_-!}\left(\frac{1}{2^N}\right) = \frac{N!}{\left(\frac{1}{2}(N+h_x)\right)!\left(\frac{1}{2}(N-h_x)\right)!}\left(\frac{1}{2}\right)^N. \tag{1.13}$$

When $N \gg 1$ and $h_x \ll Nb$, we can approximate equation (1.13) using Stirling's approximation to obtain a normalized Gaussian function of the form

$$p(h_x) = \frac{1}{\sqrt{2\pi Nb^2}}e^{-\frac{h_x^2}{2Nb^2}}. \tag{1.14}$$

The analogous distribution function $p(h)$ for a random walk in 3D is

$$p(h_x, h_y, h_z) = \left(\frac{3}{\sqrt{2\pi Nb^2}}\right)^{3/2} e^{-\frac{3}{2}\frac{h_x^2+h_y^2+h_z^2}{Nb^2}}, \tag{1.15}$$

which, once transformed using spherical coordinates, gives the final distribution function

$$p(h) = 4\pi h^2\left(\frac{3}{\sqrt{2\pi Nb^2}}\right)^{3/2} e^{-\frac{3}{2}\frac{h^2}{Nb^2}} = \frac{\Omega(h)}{\Omega_T}. \tag{1.16}$$

Of course, the distribution function yields the expected result for the mean square end-to-end distance $\langle h^2\rangle = \int_0^\infty h^2 p(h)dh = Nb^2$.

The free energy of a Freely Jointed Chain (FJC)

By definition, the configurational entropy $S(h)$ of a chain molecule is the product of the Boltzmann constant k_B with the natural logarithm of the number of conformations [8]:

$$S(h) = k_B \ln(\Omega(h)). \tag{1.17}$$

With the help of equation (1.16), we can transform equation (1.17) into

$$S(h) = S(0) - \frac{3k_B h^2}{2Nb^2} \tag{1.18}$$

where $S(0)$ is a constant corresponding to the entropy when the end-to-end distance h is zero. Since it is an ideal random walk, all conformations have the same internal energy. The free energy $F(h)$ (also called the Helmholtz free energy) can be written as

$$F(h) = U - TS(h) = F(0) + \frac{3k_B T}{2Nb^2} h^2 \tag{1.19}$$

where T is the temperature and U is the potential energy of the ideal chain (which is independent of the end-to-end distance since an ideal chain does not involve any interaction energy). Equation (1.19) has the same form as the energy of an harmonic oscillator ($E = \frac{1}{2}kx^2$). The ideal chain can thus be related to a "dumbbell" system made of two beads linked by an entropic spring of constant

$$k = \frac{3k_B T}{Nb^2} = \frac{3k_B T}{\langle h^2 \rangle}. \tag{1.20}$$

The restoring entropic force f pulling the chain ends towards each other is thus

$$f(h) = \frac{\partial}{\partial h}\left(\frac{1}{2}kh^2\right) = \frac{3k_B T}{Nb^2} h. \tag{1.21}$$

Equation (1.21) shows that the equilibrium length of the spring of the "dumbbell" is zero.

Stretching an ideal Freely Jointed Chain (FJC)

Let's consider the scenario where a constant external force f (in the x-direction) is applied on both ends of the FJC. Both ends are pulled apart along the x-axis as seen in Figure 1.5. The potential energy U of the chain in the x-direction is:

$$U = -\vec{f} \cdot \vec{h} = -fh. \tag{1.22}$$

The presence of the external force allows the conformational distribution to favor a specific $\langle \vec{h} \rangle \neq 0$. We can then calculate the partition function Z by summing the Boltzmann factors $e^{-U/k_B T}$ over all

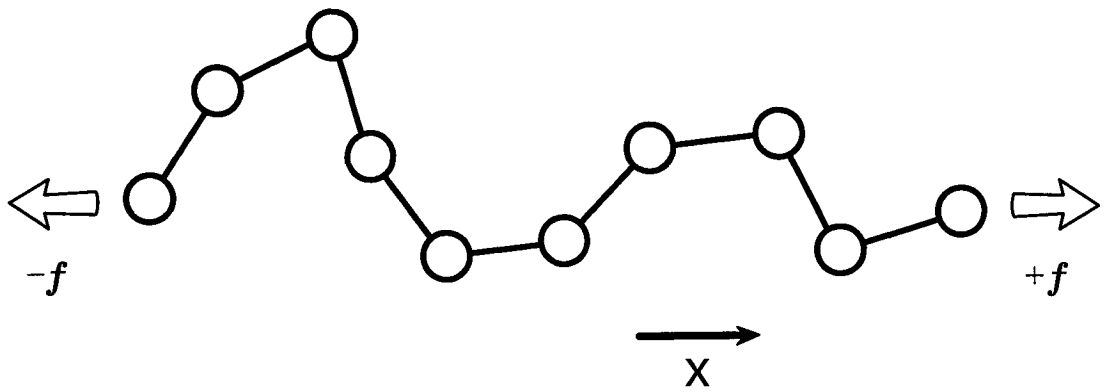

Figure 1.5: *External forces are applied on both ends of a FJC.*

possible conformations of the chain:

$$Z = \sum_{states} e^{\left(-\frac{U}{k_B T}\right)} = \sum_{states} e^{\left(\frac{fh}{k_B T}\right)}. \tag{1.23}$$

If we transform the summation into an integral over all possible bond orientations in the molecule, we get the final expression for the partition function as a function of T, f and N [8]:

$$Z(T, f, N) = \left[\frac{4\pi \sinh\left(fb/k_B T\right)}{\left(fb/k_B T\right)}\right]^N. \tag{1.24}$$

From the partition function, we can now calculate the Gibbs free energy, G, which is defined as

$$\begin{aligned} G(T, f, N) &= -k_B T \ln Z(T, f, N) \\ &= -N k_B T \left[\ln\left(4\pi \sinh\left(\tfrac{fb}{k_B T}\right)\right) - \ln\left(\tfrac{fb}{k_B T}\right)\right]. \end{aligned} \tag{1.25}$$

The Gibbs free energy is used here because the problem is considered isobaric-isothermal (constant pressure (in this case the tension f plays this role), constant temperature). The previous use of the Helmholtz free energy (Eq. 1.19) was in a problem considered isochoric-isothermal (constant extension, constant temperature).

For a given force, the average end-to-end distance h can be extracted by taking the derivative of G:

$$\langle h \rangle = -\left.\frac{\partial G}{\partial f}\right|_{N,\,T} = bN\left[\coth\left(\frac{fb}{k_B T}\right) - \frac{1}{fb/k_B T}\right]. \tag{1.26}$$

The Langevin function $\mathfrak{L}(F)$ is defined by rewriting equation (1.26) as the fractional extension (relative to $h_{\max}$) *vs.* the scaled force $F = \frac{fb}{k_B T}$ as follows [11]

$$\mathfrak{L}(F) \equiv \frac{\langle h(F)\rangle}{h_{\max}} = \coth(F) - \frac{1}{F} \cong \begin{cases} \frac{1}{3}F - \frac{1}{45}F^3 + \frac{2}{945}F^5 - O(F^7) & F \ll 1 \\ 1 - \frac{1}{F} & F \gg 1. \end{cases} \tag{1.27}$$

The result in equation (1.21) agrees with the first term in the $F \ll 1$ expansion as expected, while for the situation where $F \to \infty$, $h \to h_{\max}$, which is physically correct.

Real chains

In the ideal chain representation, the polymer is modeled by a random walk, which means that it is possible for two monomers to overlap in space. This characteristic of the ideal chain does not agree intuitively with reality. The presence of an excluded volume v_e prevents the chain monomers from completely overlapping. If we consider the situation in Figure 1.6 where a polymer chain is modeled by a series of hardcore beads, the inset shows the closest approach for two monomers. The center-to-center distance between these identical beads can only be as small as $2r_s$ since they are hard spheres. This means that the excluded volume v_e is actually 8 times the volume of one bead (for hard spheres). The actual excluded volume depends greatly on the potential used between monomers. The hard sphere case prevents all overlap while a soft sphere allows a partial overlap of monomers.

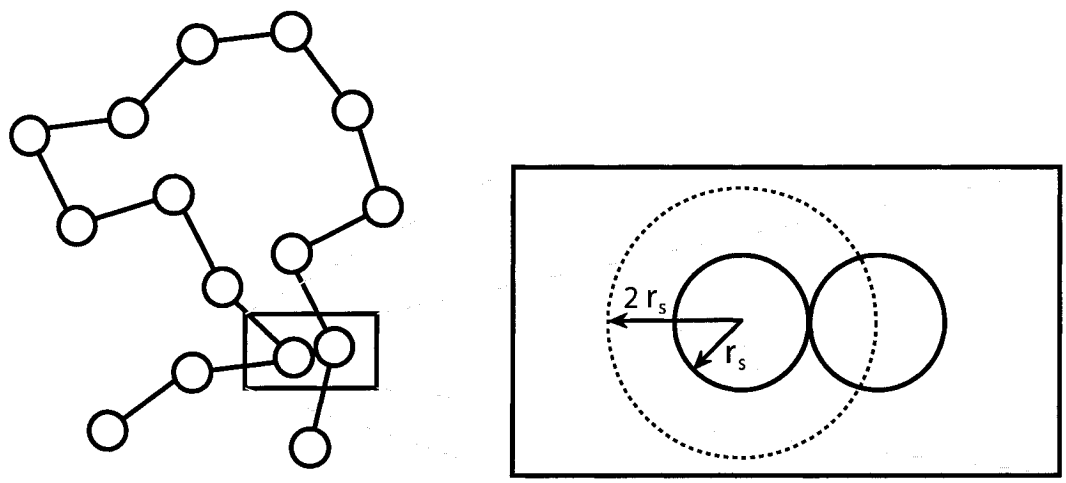

Figure 1.6: *Excluded volume in a chain molecule. The inset shows the volume which the second bead cannot enter in (dotted line).*

A major contributing factor to chain statistics is the molecular interactions between monomers. Monomers surrounded by solvent beads have the possibility to interact with other monomers of the

chain as well as with the solvent. In a good solvent the potential is the same for all the different combinations of chain monomers as well as solvent particles which, together with the excluded volume interactions, makes the chain swells more than in the ideal chain scenario. In a poor solvent, monomers in the chain are attracted more to each other than to the solvent particles. Hence a collapse of the chain occurs where the excluded volume prevents the chain from becoming a "black hole". A middle case happens when the polymer-polymer monomer attraction exactly cancels out the expansion due to the excluded volume. We then get a so-called theta solvent which, almost accidentally, gives back the same physics as the ideal chain (i.e., $\langle h^2 \rangle = Nb^2$).

Real chain in a good solvent

The excluded volume causes the mean square end-to-end distance $\langle h^2 \rangle$ to increase. This swelling leads to the well known scaling result for the end-to-end distance of an excluded volume chain [9]

$$\langle h^2 \rangle \sim N^{2\nu} b^2, \tag{1.28}$$

where ν is called the Flory exponent. For a good solvent, $\nu \cong \frac{3}{2+d}$ where d is the dimensionality of the system. For a 3D problem in a good solvent, this relation gives $\nu = 0.6$ which is very close to the experimental value of $\nu = 0.588$ (also calculated with the Renormalization Group Theory) [9].

The stretching equation (1.27) also changes when the excluded volume interactions are taken into account. As before, we look at the stretching caused by a constant force $\pm f$ applied at opposite ends, in a good solvent, but this time no exact solution can be found. However, simple scaling arguments can be applied for 4 different regimes [11]. The first regime looks at small forces, which makes the chain look like the "dumbbell" model ($f \sim kh$) with an entropic spring $k \cong \frac{k_B T}{\langle h^2 \rangle} \cong \frac{k_B T}{N^{2\nu} b^2}$ (see Fig. 1.7A):

$$\frac{\langle h \rangle}{b} \cong \frac{1}{b} \times \frac{f}{k} \cong \frac{N^{2\nu} b}{k_B T} f \cong N^{2\nu} F \sim N^{6/5} f^1 \qquad F < N^{-\nu}. \tag{1.29}$$

The second regime (called the Pincus regime) transforms the polymer into an ideal chain of N/g aligned Pincus blob of size ξ containing g monomers each (see Fig. 1.7B). The monomers inside each blob stay unperturbed by the external force f while its size $\xi = \frac{k_B T}{f}$. The scaling law for the Pincus regime [12] is

$$\frac{\langle h \rangle}{b} \cong \frac{N}{g} \times \frac{\xi}{b} \cong N \times F^{\frac{1}{\nu}-1} \sim N^1 f^{2/3} \qquad N^{-\nu} < F < 1. \tag{1.30}$$

In the third regime, $F > 1$, the chain is considered highly stretched which means that the excluded volume interactions no longer affect its end-to-end distance (see Fig. 1.7C). The chain is a FJC model

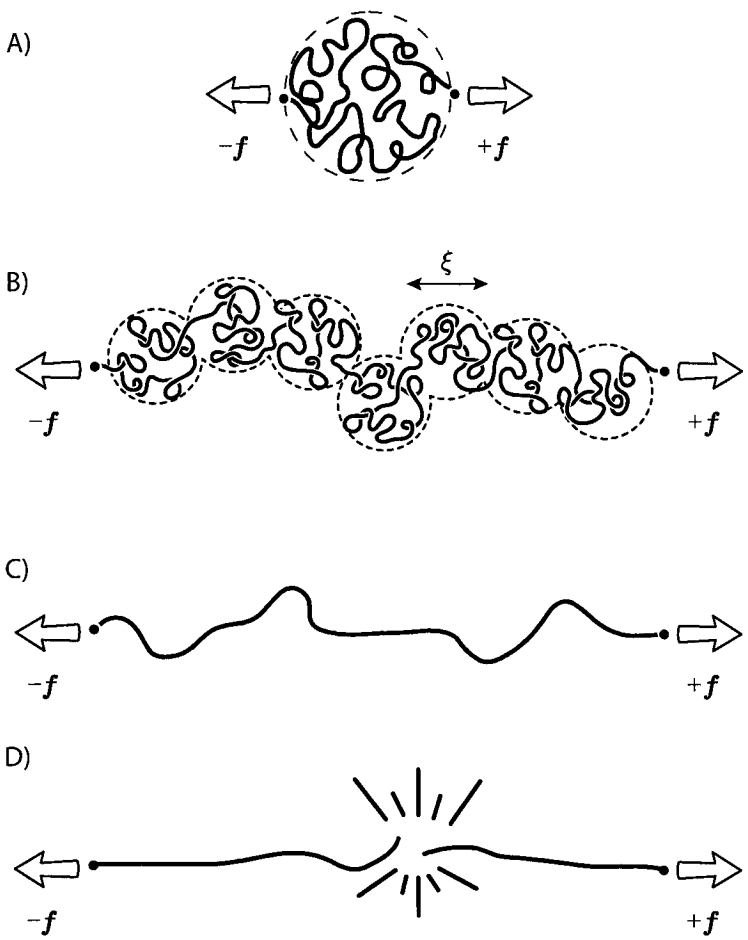

Figure 1.7: *Schematic representation of the four stretching regimes for a real chain in a good solvent. A) The chain stays undeformed. B) The Pincus blobs transform the chain into a FJC. C) The chain comes back to an ideal chain model. D) A strong applied force breaks the chain into two segments.*

which includes the highly stretched limit of the Langevin equation (Eq. (1.27)):

$$\frac{\langle h \rangle}{b} \cong N \times \left(\coth(F) - \frac{1}{F} \right) \cong N^1 \times \left(1 - \frac{1}{F} \right) \qquad F > 1. \tag{1.31}$$

The last regime occurs when the force applied to both ends is strong enough to begin stretching the chemical bonds along the backbone of the chain. In this case the average end-to-end distance $\langle h \rangle > Nb$. A chemical bond will break at a critical force and the chain will now be split into two sub chains (see Fig. 1.7D). Obviously, this regime is beyond the scope of this thesis.

Real chain in a good solvent: relaxation time

Since there is only one length scale in this problem (namely $\sqrt{\langle h^2 \rangle}$), the diffusion coefficient D needs to be defined in order to find the scaling law for the relaxation time τ_{relax} of a real chain in a good solvent (also called the Zimm relaxation time).

The diffusion coefficient D comes from the diffusion equation for the position probability function $P(x, y, z, t)$:

$$\frac{\partial P(x, y, z, t)}{\partial t} = D\nabla^2 P(x, y, z, t). \tag{1.32}$$

From the Einstein equation, the molecular diffusion coefficient is given by

$$D = \frac{k_{\text{B}}T}{\zeta}, \tag{1.33}$$

where ζ is the friction coefficient of the polymer molecule.

On the other hand, Zimm [9] determined that a polymer chain is generally non-free-draining (i.e., it does not allow solvent particles to pass through its conformation); therefore, such a hydrodynamically impermeable coil is equivalent to a hard sphere. The friction coefficient ζ of a sphere of radius h, found by Stokes, scales like

$$\zeta \sim h. \tag{1.34}$$

Since there is only one characteristic length ($\sqrt{\langle h^2 \rangle}$) in this problem and only one coefficient which explains the dynamics (the diffusion coefficient D), the scaling hypothesis predicts that the equation relating the relaxation time τ_{relax} with h and D is

$$D\tau_{\text{relax}} \cong \langle h^2 \rangle. \tag{1.35}$$

The relaxation time τ_{relax} can be seen as the time taken by the chain to diffuse over a distance of $\sqrt{\langle h^2 \rangle}$. By substituting equations (1.28), (1.33) and (1.34) into equation (1.35), one gets the following scaling law [9]:

$$\tau_{\text{relax}} \cong \frac{\langle h^2 \rangle}{D} \sim h^3 \sim N^{3\nu}. \tag{1.36}$$

Real chain in a poor solvent

To summarize, at the beginning of the section on real chains the mean-square end-to-end distance was given by the scaling law

$$\langle h^2 \rangle \sim N^{2\nu} b^2, \tag{1.37}$$

where ν is the Flory exponent. In 3D, for a good solvent, $\nu = 3/5$ while for a theta solvent, $\nu = 1/2$. Now for the poor solvent, we start from the fact that the volume of a sphere scales like r^3 (r is the radius of the sphere) or as N times the volume of one monomer. This provides us with the following relation

$$r \sim N^{1/3}, \tag{1.38}$$

which is the same type of equation seen before for a good solvent but with an exponent ν of 1/3. The exponent $\nu = 1/3$ thus characterizes those cases where the chain is in a collapsed state: a globule. One can model this globule as a collection of N/g thermal blobs of size ξ (see Fig. 1.8). Each thermal blob contains g monomers of size b that follow a random path ($\xi = g^{1/2}b$). The globule radius r_c is thus given by

$$r_c = \left(\frac{N}{g}\right)^{1/3} \xi. \tag{1.39}$$

A detailed derivation for the relation between g and the temperature T of the system can be found in the second manuscript (also in Ref. [8]).

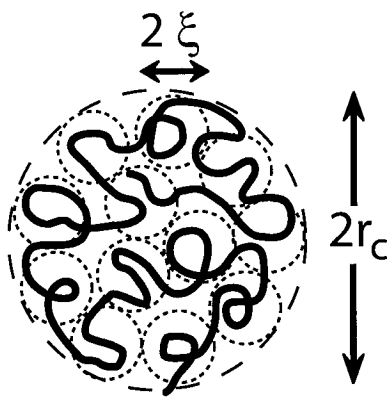

Figure 1.8: *A schematic picture of the chain in a collapsed state. The globule is made of small thermal blobs (dotted lines) of size ξ.*

Shear flow

The definition of a shear rate $\dot{\gamma}$ is

$$\dot{\gamma} \equiv \frac{\Delta V}{\Delta r} \tag{1.40}$$

where V is a velocity in the direction of the flow and r corresponds to a position perpendicular to the shear flow. Figure 1.9 shows an example of a shear flow. The bottom wall is fixed in space while the top

wall moves at a constant speed which creates a uniform shear flow with help from the friction between the moving wall and the solvent particles. In this case, the shear rate $\dot{\gamma}$ between the walls is uniform and it is given by the difference between the velocity at the top wall (V) and the velocity at the bottom wall (0), divided by the distance between the walls.

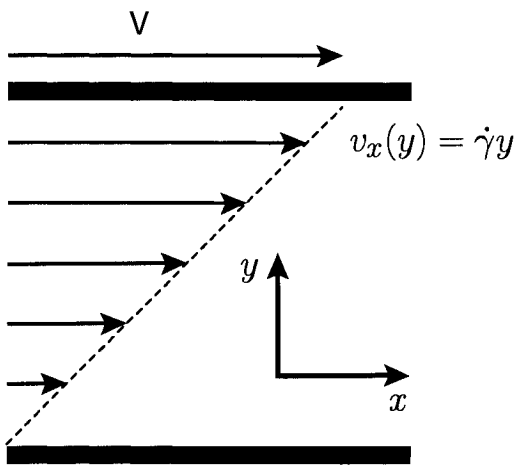

Figure 1.9: *Diagram of a system with a shear flow.*

1.2 Past studies

In this section, we review articles (in chronological order) from two groups of researchers who have previously worked on the type of problem tackled in this thesis. Although it is not an exhaustive review, it will point the interested reader to relevant material.

Brochard-Wyart and co-workers

In 1993, Brochard-Wyart developed a new theory of chain stretching [13]. The author looked at the conformations of flexible chains (tethered by one end to a wall) in a good solvent that are being stretched by two types of flow: a strong uniform flow of velocity V and a shear flow $V_x(y) = \dot{\gamma}y$. One of the main points of the article was the investigation of a novel stretching regime, known as the *trumpet* regime.

If we take for example the case of a uniform flow in the x-direction just strong enough to stretch the coiled chain, the author demonstrated that the chain could be described by a string of Pincus blobs decreasing in size from the free end to the tethering point (see Fig. 1.10A). The height of these blobs,

$y(x)$, scales like

$$y(x) \sim \frac{R_1^2}{x}, \tag{1.41}$$

where R_1 is the radius of the largest (terminal) blob and x is the distance in the direction of the uniform flow relative to the free end. The inverse proportionality between y and x makes the envelope modulating the height of the blobs look like a *trumpet*. The theoretical prediction for the chain span s is

$$s \cong N^3 b^5 \left(\frac{\eta V}{k_B T}\right)^2 \sim V^2, \tag{1.42}$$

where N is the number of monomers in the chain, b is the monomer size, η is the solvent viscosity, k_B is Boltzmann's constant and T is the temperature.

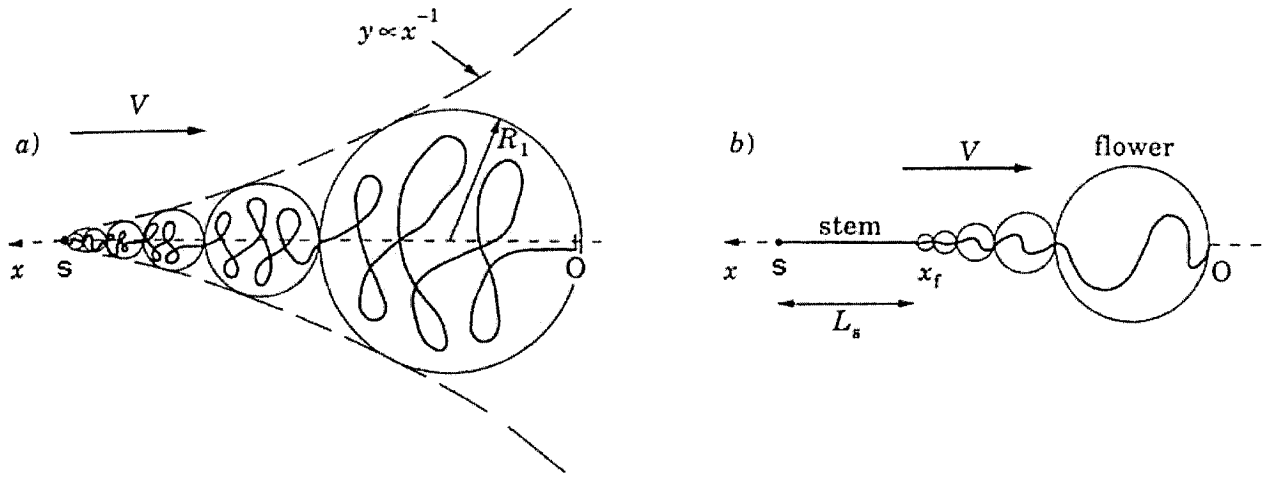

Figure 1.10: *Deformation of a tethered chain under uniform flows. A) Trumpet regime. B) Stem and flower regime. (Taken from Ref. [14], Fig. 1).*

For the other type of flow (shear flow $V_x(y)$), a chain tethered to a hard surface can be represented by a string of Pincus blobs which decrease in size from the free end to the tethered point (see Fig. 1.11), but this time the height of the blobs scales like

$$y(x) \sim \frac{R_1^{3/2}}{\sqrt{x}}. \tag{1.43}$$

Again the relation between y and x gives rise to a trumpet shape. The chain span s in a shear flow is

$$s \cong N^{3/2} b^{5/2} \left(\frac{\eta \dot{\gamma}}{k_B T}\right)^{1/2} \sim \dot{\gamma}^{1/2}, \tag{1.44}$$

where $\dot{\gamma}$ is the shear rate.

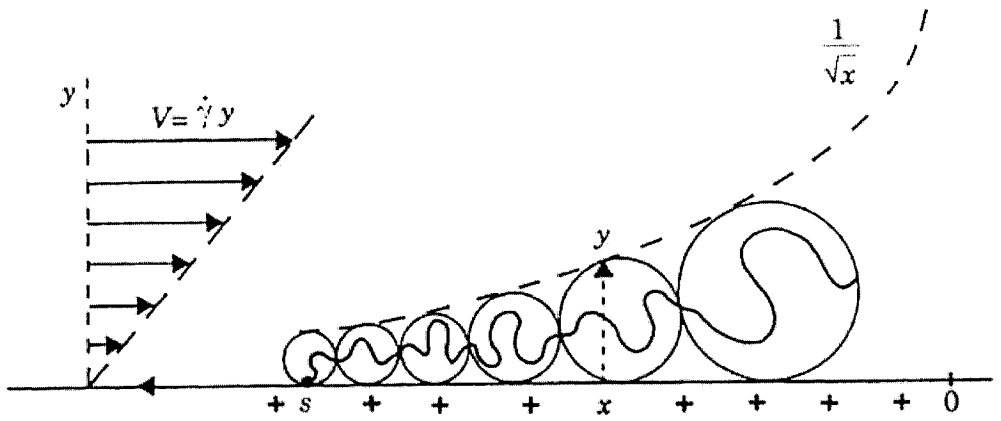

Figure 1.11: *Deformation of a tethered chain in a shear flow. (Taken from Ref. [13], Fig. 3)*

In 1995, Brochard-Wyart [14] developed an additional theory for stronger uniform flows in order to explain the experimental results of Perkins *et al.* [15]. This regime, the *stem and flower* regime, divides the chain in two parts: the stem of diameter b and length L_s, and the flower at the free end (see Fig. 1.10B). The addition of the stem length to the flower size gives a chain span s of

$$s \cong Nb - \frac{2}{3}\frac{k_B T}{\eta b V} \tag{1.45}$$

where the coefficient 2/3, although approximate, was kept to indicate how fast the span changes with the velocity.

A year later, Buguin and Brochard-Wyart [16] extended this work to include collapsed chains in poor solvents. The authors divide the uniform flow range in three regimes. In the first regime, the collapsed chain looks like a collapsed globule. The second regime, as seen in Figure 1.12, separates the chain into two parts: a stem of length L_s and a globule of size L_g. The chain span for this case is

$$s \cong L_g e^{\left[\frac{\eta V b^2}{k_B T}(N-n^*)\right]}, \tag{1.46}$$

where n^* is the number of monomers in the globule.

In the third regime the globule disappears and the chain becomes fully elongated ($s \cong Nb$).

The case of the collapsed chain tethered to a wall in a shear flow was also studied theoretically by Buguin and Brochard-Wyart [16]. We will not describe it in this section since this topic is covered extensively in Chapter 3 of this thesis.

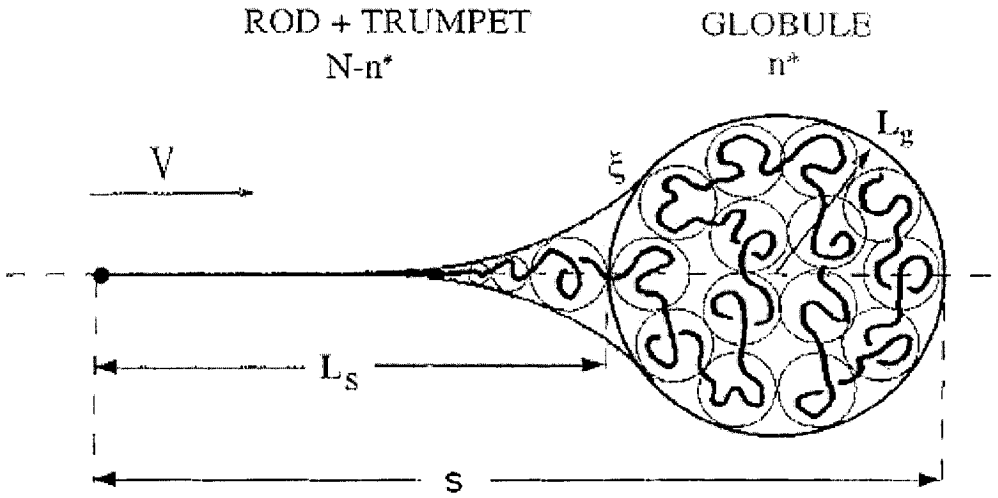

Figure 1.12: *Schematic representation of a collapsed chain deformation in a uniform flow. (Taken from Ref. [16], Fig. 4)*

Doyle and co-workers

In 2000 Doyle *et al.* [5, 7] published two articles studying the dynamics of polymers tethered to a surface in a shear flow and a good solvent. Together, these articles provide experimental results in combination with a new theory and Brownian Dynamics simulations.

Since the theory for the strong shear flow regime is covered in Chapter 2 of this thesis, we only present a brief overview, with a few clarifications. The aim of this model is to find a scaling law for FJC and WLC polymers which relates the unstretched fraction ε (i.e., $\varepsilon = 1 - h/h_{\max}$) to the shear rate $\dot{\gamma}$. Four basic principles are at the heart of the model. First, a polymer stretched by a constant force in the x-direction has fluctuations in the transverse y-direction of δy (see Fig. 1.13). One can calculate the restoring force $F(\delta y)$ in the y-direction via simple algebra [17]

$$F(\delta y) = \sin(\theta) F(h) = \frac{\delta y}{\sqrt{x^2 + \delta y^2}} F\left(\sqrt{x^2 + \delta y^2}\right). \tag{1.47}$$

A first order approximation of equation (1.47) gives

$$F(\delta y) \cong \left(\frac{F(x)}{x}\right) \delta y. \tag{1.48}$$

Equation (1.48) looks like Hooke's law with spring constant $k_\perp$ (in the transverse direction):

$$k_\perp = \frac{F(x)}{x}. \tag{1.49}$$

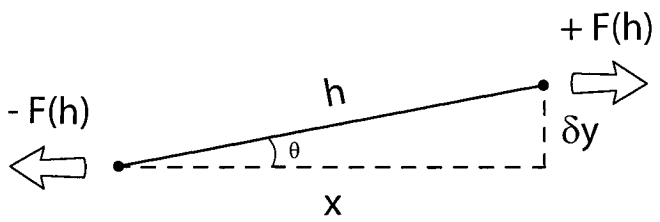

Figure 1.13: *Schematic representation of a chain mostly stretched in one direction.*

The authors use equation (1.49) and the equipartition theorem for the transverse thermal fluctuations of the chain, in conjunction with the balance between the friction force and the spring force (Langevin equation (1.27) for FJCs; and the Marko and Siggia equation [18] for the WLC) to extract the following scaling laws:

$$\varepsilon_{\mathrm{FJC}} \sim \dot{\gamma}^{-2/3} \tag{1.50}$$

and

$$\varepsilon_{\mathrm{WLC}} \sim \dot{\gamma}^{-1/3}. \tag{1.51}$$

These scaling laws neglect the effect of hydrodynamic interactions in two instances: between individual monomers and between monomers and the surface. A constant drag coefficient is also assumed.

To validate equations (1.50) and (1.51), Doyle *et al.* utilized Brownian Dynamics simulations. They modeled the chain as a linear spring attached at one end to a surface and at the other end to a single Brownian bead. The equations of motion of the bead in the directions perpendicular to the flow (y and z) are the same as an harmonic potential with thermal fluctuations, but with no influence from the shear flow in the x-direction. On the other hand, the velocity of the bead in the flow direction is dependent on $k_{\perp}$, the thermal fluctuations, and on the shear flow. Figure 1.14 shows a good agreement between the predicted scaling laws for FJC and WLC and the Brownian dynamics simulations. The Weissenberg number Wi is the dimensionless shear flow strength defined as the product between the shear rate, $\dot{\gamma}$, and the longest relaxation time, τ_{relax}, of the chain.

Furthermore, Doyle *et al.* used an experimental setup [5, 7] like the one depicted in Figure 1.15 to experimentally verify their new chain stretching theory. The channel size was 100 μm in width by 200 μm in height by 2.5 cm in length. An inverted microscope equipped with an oil immersion objective was placed under a coverslip coated with streptavidin. Three lengths of λ-phage DNA chains were used:

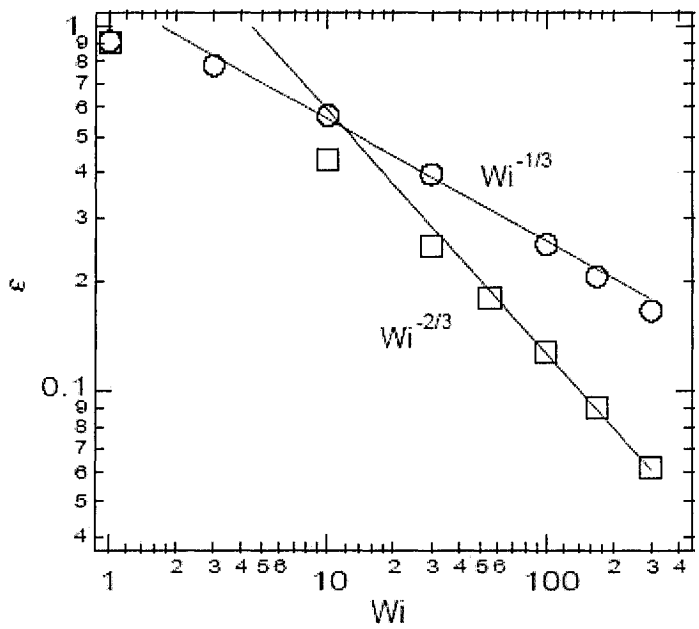

Figure 1.14: *Comparison of predicted scaling laws with Brownian Dynamics simulations for a WLC (circles) and FJC (squares). The simulations are for chains with 357 Kuhn steps (two λ DNA molecules ligated together). (Taken from Ref. [7], Fig. 2)*

48 kbp (λ), 96 kbp (2λ) and 144 kbp (3λ). Some modifications are made to the DNA chains. Each DNA chain is hybridized and ligated with T4 DNA ligase. Also, to actually see the conformations of the DNA chains, they are fluorescently labeled with YOYO-1 dye at a ratio of one dye molecule per eight base pairs. The λ-phage DNA has a biotinylated oligonucleotide (complimentary to the 12 base pair overhang of the chain) ligated to the end of the molecules. A shear flow created by a syringe pump stretches the tethered DNA chains. An argon-ion laser is used with a wavelength of 488 nm to excite the fluorescent DNA molecules. The fluorescent light is captured by a cooled intensified CCD camera. The experiments were performed at 24 °C in pH 8.3 TBE buffer.

To get the longest relaxation time τ_{relax}, the chains are initially stretched by a shear rate of 57 s^{-1}. The flow is then stopped. An exponential fit of the data after the chain's extension gets to one third its contour length provides a value for τ_{relax}. Fifteen chains per chain length were used to obtain the relaxation time τ_{relax}: $\tau_\lambda = 0.45$ s, $\tau_{2\lambda} = 1.45$ s, $\tau_{3\lambda} = 2.56$ s.

Figure 1.16 shows actual conformations of λ-phage DNA chains for different values of Wi. The interesting point is the large conformational fluctuations that the chain undergoes for intermediate Wi (=5.1). These fluctuations occur in the predicted Wi range where a cyclic motion of the chain is

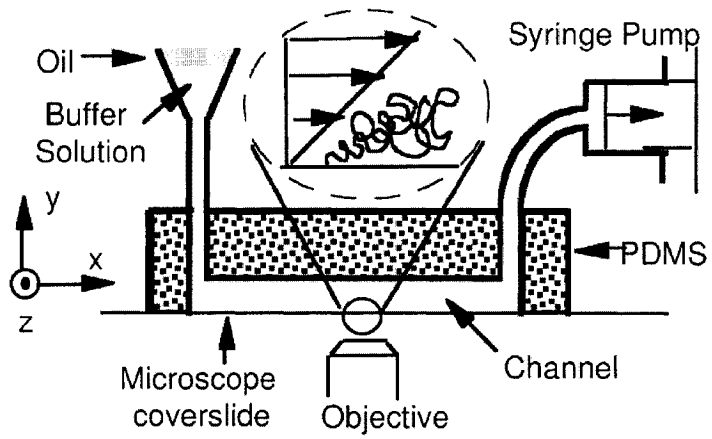

Figure 1.15: *Schematic representation of the experimental apparatus used by Doyle, Ladoux and Viovy [5]. (Taken from Ref. [5], Fig. 1)*

thought to exist (which will be discussed later in this section).

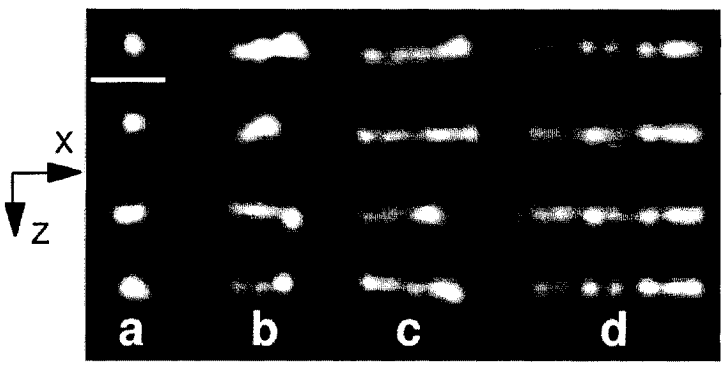

Figure 1.16: *Time series (top to bottom) of the configurations of λ-phage DNA molecules at varying flow strengths obtained with the experimental setup shown in Fig. 1.15. The horizontal scale bar in A is 5μm. In each series, the images are separated by an interval of* τ_{relax}*: A) equilibrium (*$Wi = 0$*); B)* $Wi = 5.1$*; C)* $Wi = 14.5$*; D)* $Wi = 110$*. (Taken from Ref. [5], Fig. 2)*

The mean fractional extension (visual length in the direction of the shear flow divided by theoretical contour length) provides us with a quantitative measure of the chain deformation. In Figure 1.17A, each data point corresponds to 40 seconds of time averaged for 10 separate chains. All three curves are superposed. As a general observation, a rapid increase in mean fractional extension occurs from $Wi = 0$ to $Wi \sim 20$. At $Wi \sim 20$, the chains are all extended over 50% of their respective contour length, while for large Wi, the increase in mean fractional extension diminishes dramatically.

It is clear from Figure 1.17B that the chain extensions tend asymptotically toward their contour

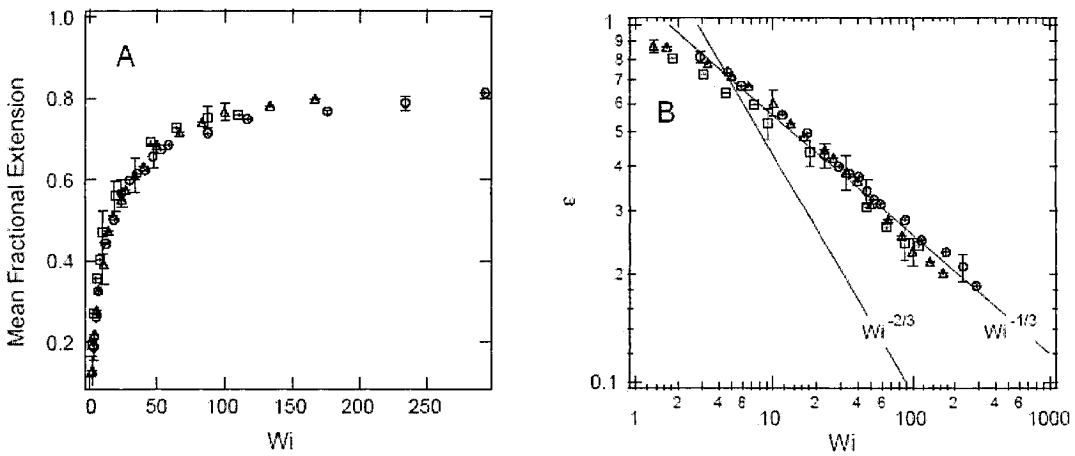

Figure 1.17: *A) Mean fractional chain extension vs. Wi: λ (squares), 2λ (triangles), and 3λ (circles). (Taken from Ref. [7], Fig. 5) B) Comparison of experimental data in a log-log plot to the predicted scaling laws for the FJC and WLC models. (Taken from Ref. [7], Fig. 6)*

lengths. The scaling laws for FJC and WLC are added to Figure 1.17B in order to compare with the experimental data. It is without any doubt that the DNA chains are WLC since the scaling law is in good agreement with the experimental data for all three chain lengths for strong shear flows.

In the region of high conformational fluctuations ($Wi \sim 5$), recirculating motions (or cyclic dynamics) occurs. An example of this type of motion is shown in Figure 1.18. Section C) of the figure shows five chain conformations which correspond to points indicated in B). The starting point of the cycle in this example is a conformation of the chain where it is not fully elongated while being close to the surface (C1). A fluctuation will bring it into stronger flow (C2) from which will follow a rapid increase in the chain extension (C3). The chain will then rotate slowly towards the surface like a lever (C4). Now close to the wall, the chain is no longer in strong shear flow, so it will relax to a compact state (C5) similar C1. It was found through the power spectrum of the simulated chain extension that the cyclic motion does not seem to have a specific cycling time, but rather a broad distribution of cyclic times.

1.3 Simulation details

To model the intermolecular interactions in liquids or dense fluids, one must construct a potential that includes two parts: an attractive term and a repulsive term. Mie [19] in 1903 was the first to propose

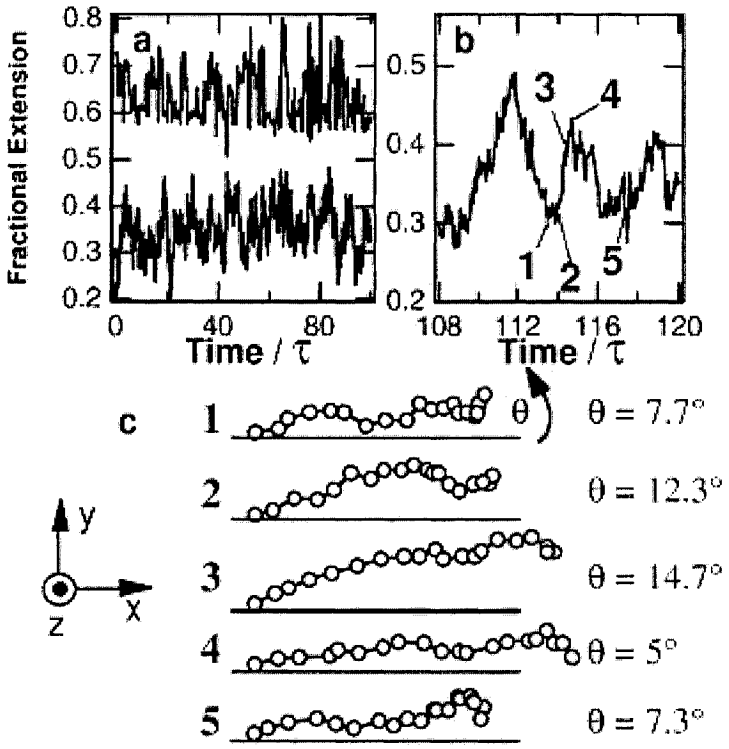

Figure 1.18: *Results from simulations for $Wi = 5.1$. A) Temporal chain fluctuations for simulations (bottom data set) and sample experimental data (top data set displaced by 0.4 for clarity). B) Temporal chain fluctuations (zoom). C) Cyclic chain dynamics. The five different configurations correspond to the points indicated in B). The angle θ is the orientation of the vector joining the tethering point to the center of mass of the chain, with regards to the tethering surface. (Taken from Ref. [5], Fig. 5)*

an empirical general interaction pair potential U_{Mie} that includes both features:

$$U_{\text{Mie}} = \left(\frac{A}{r_{ij}}\right)^m - \left(\frac{B}{r_{ij}}\right)^n, \tag{1.52}$$

where r_{ij} is the distance between the centers of molecule i and j, m and n are positive integers, and A and B are constant.

One special case of Mie's potential is the well known Lennard-Jones (LJ) potential U_{LJ} [20, 21] which is defined as

$$U_{\text{LJ}} = 4\epsilon\left[\left(\frac{\sigma_{\text{LJ}}}{r_{ij}}\right)^{12} - \left(\frac{\sigma_{\text{LJ}}}{r_{ij}}\right)^{6}\right] \tag{1.53}$$

where the energy ϵ corresponds to the depth of the well and σ_{LJ} is the characteristic distance. The term $\left(\frac{\sigma_{\text{LJ}}}{r_{ij}}\right)^{12}$ plays the part of the steep repulsive wall at distances $r_{ij} \leq \sigma_{\text{LJ}}$ while the term $\left(\frac{\sigma_{\text{LJ}}}{r_{ij}}\right)^{6}$ creates the long-range attractive tail.

For simulation efficiency we cutoff the Lennard-Jones potential at a distance r_{cut}. The cutoff creates

a discontinuity in the force and in the actual motion. To compensate, U_{LJ} is often shifted by a specific amount of energy. The cutoff shifted potential U_{LJ} (see Fig. 1.19A) is then described by the following equation:

$$\begin{aligned} U_{\mathrm{LJ}}(r_{ij}) &= 4\epsilon\left[\left(\frac{\sigma_{\mathrm{LJ}}}{r_{ij}}\right)^{12} - \left(\frac{\sigma_{\mathrm{LJ}}}{r_{\mathrm{cut}}}\right)^{12} - \left(\frac{\sigma_{\mathrm{LJ}}}{r_{ij}}\right)^{6} + \left(\frac{\sigma_{\mathrm{LJ}}}{r_{\mathrm{cut}}}\right)^{6}\right]; r_{ij} < r_{\mathrm{cut}} \\ &= 0; \qquad r_{ij} \geq r_{\mathrm{cut}}. \end{aligned} \tag{1.54}$$

In the first manuscript of this thesis (Chapter 2), we use a repulsive LJ potential (i.e., $r_{\mathrm{cut}} = 2^{1/6}\sigma_{\mathrm{LJ}}$;

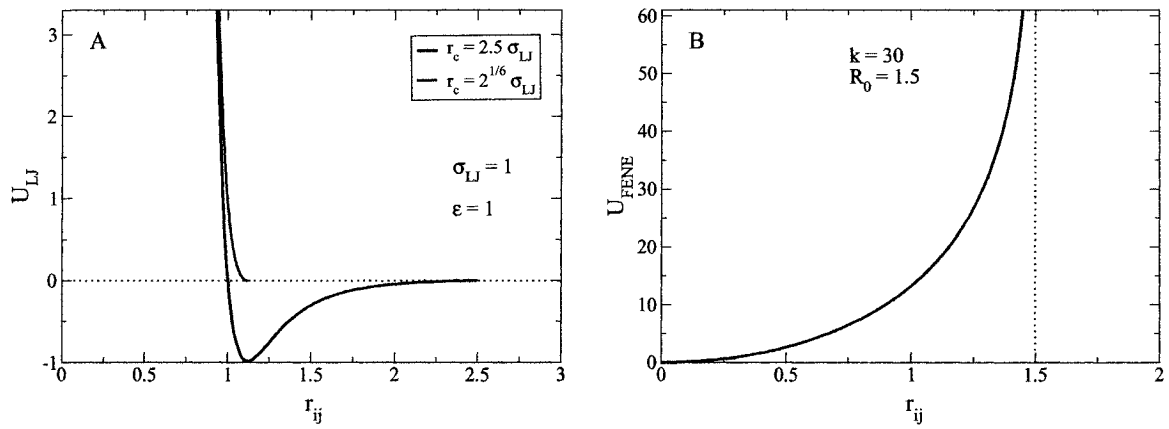

Figure 1.19: *A) Examples of two shifted Lennard-Jones potentials (full line is $r_{\mathrm{cut}} = 2.5\sigma_{\mathrm{LJ}}$; dotted line is $r_{\mathrm{cut}} = 2^{1/6}\sigma_{\mathrm{LJ}}$). B) Example of a Finitely Extensible Nonlinear Elastic (FENE) potential. The dotted lines are a visual aid in both cases.*

see dotted line in Fig. 1.19A), while for the second manuscript (Chapter 3), a LJ potential with the attractive part is used (i.e., $r_{\mathrm{cut}} = 2.5\sigma_{\mathrm{LJ}}$; see full line in Fig. 1.19A).

To link consecutive monomers in a chain, another potential must be used. An important characteristic of this potential is that it must provide an upper bound for the bond length between the consecutive monomers of the chain. The use of a harmonic potential, for example, does not provide such an upper bound. Figure 1.19B shows that the Finitely-Extensible Nonlinear Elastic (FENE) potential [22, 23] fits the maximum bond length criterion. The equation for the FENE potential is

$$U_{\mathrm{FENE}} = -\frac{1}{2}kR_0^2 \log\left(1 - \frac{r_{ij}^2}{R_0^2}\right); \qquad r_{ij} < R_0, \tag{1.55}$$

where we generally choose $k = 30\epsilon/\sigma_{\mathrm{LJ}}^2$ and $R_0 = 1.5\sigma_{\mathrm{LJ}}$.

In our simulations, we represent the monomers of the chain as well as the solvent particles by beads which interact via the LJ potential, while consecutive monomers in the chain are bound together by

the FENE potential. We use the Molecular Dynamics (MD) scheme [24, 25] (with the velocity Verlet algorithm [26]) to solve Newton laws of motion for the beads. We typically determine the equilibrium and dynamic properties of the system from time averages taken over sufficiently long time intervals.

The classic example which is used to illustrate the actual magnitude of the LJ potential is liquid argon. Since it is a uncharged one-atom molecule, it is fair to represent one argon atom by a uncharged bead. The argon LJ potential parameters are [20, 21]:

$$\begin{aligned} &\text{the energy} && \epsilon = 120\,^{\circ}K k_{\mathrm{B}} \cong 2 \times 10^{-21}\mathrm{m}^2\,\mathrm{kg}\,\mathrm{s}^{-2}, \\ &\text{the length} && \sigma_{\mathrm{LJ}} = 3.4 \times 10^{-10}\mathrm{m}, \text{ and} \\ &\text{the mass} && m = 39.95/N_{\mathrm{A}} \cong 6 \times 10^{-26}\mathrm{kg} \end{aligned}$$

where N_{A} is Avogadro's number. In MD simulations, the discretization of the equations of motion yield to a fundamental time step τ_{LJ} which equals to

$$\tau_{\mathrm{LJ}} = \sigma_{\mathrm{LJ}}\sqrt{\frac{m}{\epsilon}} \sim 10^{-12}\mathrm{s}. \tag{1.56}$$

The main advantage of MD simulations (which include solvent) is that hydrodynamic interactions (HI) and excluded volume interactions are implicitly taken into account in the system. Other simulation methods like Metropolis Monte-Carlo (MC) or Brownian Dynamics do not include HI. The disadvantage of MD is that obtaining thermodynamic average is computationally expensive. For an MD simulation with $r_{\mathrm{cut}} = 2.5\sigma_{\mathrm{LJ}}$ and 36000 beads, good averages in a nonequilibrium system can be obtained in weeks while an equivalent system without HI like MC takes hours to produce results on the same computer.

Since the computing demand was really high to get good averages for our MD simulations, we used the following super-computers to accelerate the process: the High Performance Computing Virtual Laboratory (HPCVL), the Shared Hierarchical Academic Research Computing Network (SHARCNET) and the Western Canada Research Grid (WestGrid).

1.4 Presentation of the thesis

The core of this thesis in made of two manuscripts:

Y. Gratton and G. W. Slater

Molecular Dynamics Study of Tethered Polymers in Shear Flow. *Accepted for publication in the European Physical Journal E (June 13, 2005).*

In the first manuscript, we use Molecular Dynamics (MD) simulations to study the dynamics of a single chain tethered by one end to a surface in shear flow. We find that Ladoux and Doyle theory for

tethered chains in strong shear flows agrees with our simulation results. We propose an approximate interpolation formula which agrees with current theories and appears to apply for simulation data for both weak and strong flows. We look at the dynamics of the cyclic motion of the chain and we investigate the influence of the chain on the flow profile.

Y. Gratton and G. W. Slater

Molecular Dynamics Study of Collapsed Tethered Polymers in Shear Flow. *To be submitted to European Physical Journal E.*

In the second manuscript, we study the same problem but with a poor solvent instead of a good one. We present a simplified theory, based on those of Buguin and Brochard-Wyart [16] for collapsed tethered chains, which agrees with our simulation results. No cyclic motion of the chain is found as expected, but other interesting dynamical properties are observed. We observe the presence of discrete preferred span lengths of the chain at intermediate shear flows. We also report on a hysteretic behavior of the chain span in time-dependent flows.

1.5 Other contributions

During my Master program, I contributed to other publications beyond the two manuscripts which make the core of this thesis. I also presented my work at two conferences. Here is a summary of these activities:

Articles

- G. W. Slater, **Y. Gratton**, M. Kenward, L. McCormick, and F. Tessier,
  Deformation, Stretching and Relaxation of Single Polymer Chains: Fundamentals and Examples.
  Soft Materials, 2003, 1, 365–391.

- M. Kenward, F. Tessier, Y. Tatek, **Y. Gratton**. S. Guillouzic, and G. W. Slater,
  Molecular Dynamics Simulations of Polymers in Micro-environments.
  in *Proceedings of the* 17^{th} *International Symposium on High Performance Computing Systems and Applications and OSCAR Symposium*, (David Sénéchal, editor), NRC Research Press, 2003, 47–55.

- G. W. Slater, S. Crişan, and **Y. Gratton**,
  Stretching and Relaxation of a Polymer Chain.
  Physics in Canada, 2003, March/April, 59, 57–66.

Book chapters

- G. W. Slater, **Y. Gratton**, M. Kenward, L. McCormick, and F. Tessier,
  Deformation, Stretching and Relaxation of Single Polymer Chains: Fundamentals and Examples.
  in *Soft Materials: Structural and Dynamics*, (John Dutcher and Alejandro G Marangoni,editors),
  Deker/CRC Press, 2004, pp. 73–105.

American Physical Society Annual Meeting

- Poster Presentation: March 2004 (Montréal),
  Molecular dynamics study of tethered polymers in shear flow: freely jointed and worm like chains.
  Yannick Gratton and Gary W. Slater.
  Session K1, poster 227.
  http://www.aps.org/meet/MAR04/baps/abs/S3610227.html

75th Annual Meeting of The Society of Rheology

- Poster Presentation: October 2003 (Pittsburgh),
  Molecular dynamics of a polymer tethered to a solid surface in a flow.
  Yannick Gratton and Gary W. Slater.
  Poster PO59.
  http://www.rheology.org/sor03a/abstract.asp?PaperID=269

1.6 Statement of originality

The work presented in this thesis has not previously been submitted for a degree or diploma in any university. To the best of my knowledge and belief, the thesis is new and original, containing no material previously published or written by another person except where due reference is made in the thesis itself. I developed all the original ideas, with crucial input from my supervisor Gary W. Slater. I wrote the two papers presented next, with critical proof reading by Dr. Slater.

Article I

Molecular Dynamics Study of Tethered Polymers in Shear Flow.

Y. Gratton and G. W. Slater

Accepted for publication in the European Physical Journal E (June 13, 2005).

2 Theory

Ladoux and Doyle [4] have proposed a simple theoretical model to explain the stretching of tethered FJC and Worm Like Chains (WLC) in a shear flow (Fig. 1). Let us first review the model as applied to the FJC case. This theory is based on four basic principles. First, for small chain extensions, the entropic restoring force behaves essentially like a spring in both directions (parallel and perpendicular to the flow). On the other hand, for large extensions [5] one can determine (using a simple geometric argument) that the transverse harmonic spring constant $k_\perp$ is equal to an effective parallel harmonic spring constant $k_\parallel^0$ given by:

$$k_\perp = k_\parallel^0 = \frac{F_x}{h_x} = \frac{f_x}{h_x} \times \frac{k_B T}{b} \tag{1}$$

where F_x is the chain restoring force in x (where x is parallel to the flow direction), f_x is the dimensionless force, b is the mean bond length, k_B is the Boltzmann constant, T is the temperature and h_x is the corresponding chain extension. We must stress the fact that equation (1) is in fact valid only for the type of problems examined in this article where $h_x \to h_{\max} \cong Nb$ (N is the number of monomers in the chain). Second, the polymer experiences thermal motion in the direction (z) transverse to the wall. This motion is assumed to satisfy the equipartition law

$$\frac{1}{2} k_\perp \delta z^2 = \frac{1}{2} k_B T, \tag{2}$$

where δz^2 is the variance of the chain's transverse fluctuations. Third, because the polymer is highly stretched by the shear flow, it tends to be free draining, which implies that intramolecular hydrodynamic interactions are negligible. Consequently, the force is related to the friction via the standard relation

$$f_x \cong \zeta_R \dot{\gamma} \delta z, \tag{3}$$

where $\dot{\gamma}$ is the shear rate and ζ_R is the friction coefficient of the chain. We note that in a free-draining regime, ζ_R simply scales like the number of monomers in the chain (N) times the friction coefficient of one monomer ($\simeq \eta b$). Fourth, the FJC model has a well known exact solution (the Langevin function) which relates the extension, the maximum extension $h_{\max}$, and the force. For $f_x \gg k_B T/b$,

$$\frac{1}{f_x} \cong 1 - \frac{h_x}{h_{\max}} \equiv \varepsilon. \tag{4}$$

This defines ε as the unstretched polymer fraction. One way to quantify a shear flow in a system is through the dimensionless Weissenberg number $Wi \equiv \dot{\gamma}\, \tau_{\text{relax}}$, the product of the shear rate $\dot{\gamma}$ and the longest (equilibrium) relaxation time of the polymer τ_{relax}. To be more specific we use the end-to-end distance relaxation time for τ_{rclax}. In theory τ_{relax} scales like $N^{3\nu}$ where $\nu = \frac{3}{5}$ [6]. Finally, by manipulating equations (1)–(4) one can derive the scaling law between ε and Wi for a FJC:

$$\varepsilon \sim \frac{N^{1/5}}{Wi^{2/3}}. \tag{5}$$

The same logic and principles can be used for the WLC. The large force approximation proposed by Marko and Siggia [7] then replaces equation (4) by $f_x \sim \varepsilon^{-2}$, and the WLC scaling law becomes

$$\varepsilon \sim \frac{N^{1/10}}{Wi^{1/3}}. \tag{6}$$

Ladoux and Doyle [4] tested their WLC model experimentally with ligated λ-phage DNA chains. They found a good agreement between the scaling model and the experimental data for three different DNA lengths, as well as a good agreement between the FJC predictions and their corresponding Brownian Dynamics (BD) simulations. We provide a computational test of the theory for a FJC below which includes Hydrodynamic Interactions (HI).

3 Molecular Dynamics Model

The system is bounded in the z-direction by two surfaces made of a single sheet of beads while periodic boundary conditions are applied in the x and y directions. The polymer is made of $N = 20$, 30 or 40 beads and the first bead is embedded in the middle of the bottom wall (see Fig. 1). The system has dimensions $2.5N\sigma_{\text{LJ}} \times 20\sigma_{\text{LJ}} \times 20\sigma_{\text{LJ}}$ in the x, y, and z directions respectively, where σ_{LJ} is the length scale of the Lennard-Jones potential (see Eq. (7)). The solvent particles are represented by united-atom beads that fill out the volume between the walls with a system density $\rho = 0.85\sigma_{\text{LJ}}^{-3}$.

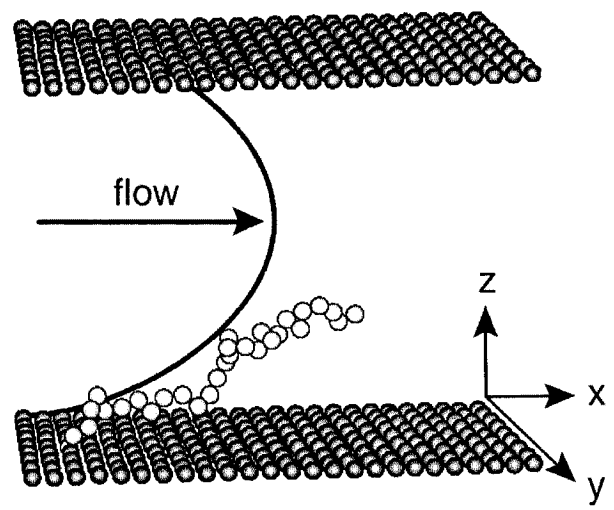

Fig. 1. *A schematic picture of the system investigated in this article. The FJC polymer chain is attached to the bottom wall and stretches out in response to the strong shear flow.*

All beads in the system interact via the *repulsive* part of the Lennard-Jones potential [8,9] (also called a Weeks-

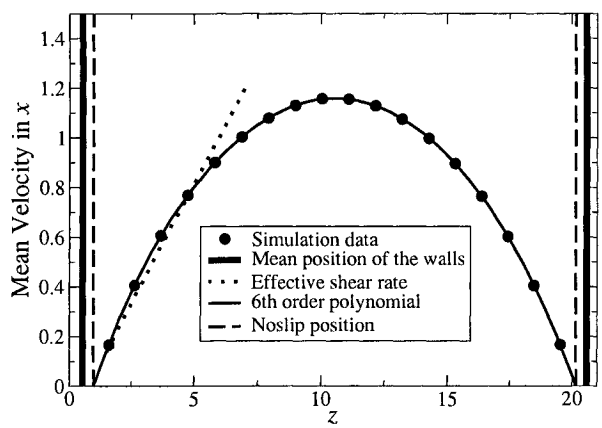

Fig. 2. *The mean flow profile between the two solid walls for an external driving force $F_g = 0.06$. The effective shear rate is defined as the average slope of the velocity curve between the bottom wall and the mean position of the last bead of the chain. The mean z-position of the center of mass of the wall beads is shown by the two thick vertical lines. The no-slip planes (dashed vertical lines) are found at positions $\Delta z = 0.50\sigma_{\rm LJ}$ from the two walls for this example. The data points were fitted using a sixth-order polynomial.*

Chandler-Anderson (WCA) potential)

$$U_{\rm wca}(r_{ij}) = 4\epsilon\left[\left(\frac{\sigma_{\rm LJ}}{r_{ij}}\right)^{12} - \left(\frac{\sigma_{\rm LJ}}{r_{ij}}\right)^{6} + \frac{1}{4}\right]; \; r_{ij} < r_{\rm cut} \quad (7)$$
$$= \qquad 0; \qquad\qquad r_{ij} \geq r_{\rm cut}$$

where r_{ij} is the distance between the centers of beads i and j. The characteristic distance $\sigma_{\rm LJ}$ and energy ϵ are set to 1, and the cutoff is $r_{\rm cut} = 2^{1/6}\sigma_{\rm LJ}$. Consecutive beads along the linear polymer chain are attached by a Finitely Extensible Nonlinear Elastic (FENE) potential [10,11]

$$U_{\rm FENE} = -\frac{1}{2}kR_0^2 \log\left(1 - \frac{r_{ij}^2}{R_0^2}\right), \qquad r_{ij} < R_0 \quad (8)$$

where $k = 30\epsilon/\sigma_{\rm LJ}^2$ and $R_0 = 1.5\sigma_{\rm LJ}$. The beads forming the wall are bound in place by a simple harmonic potential

$$U_w = \frac{1}{2}k_w {r_w}^2 \quad (9)$$

where $k_w = 120\epsilon/\sigma_{\rm LJ}^2$ and r_w is the distance between the reference position for a bead (its mean position on the wall simple square lattice structure which has a 1.06σ inter-lattice spacing) and its actual position. In the rest of this article, we report numerical values in the standard MD units of length $\sigma_{\rm LJ}$ and time $\tau_{\rm LJ} = \sigma_{\rm LJ}\sqrt{m/\epsilon}$, where m is the mass of a bead. In equilibrium the mean bond length is $b = 0.97$.

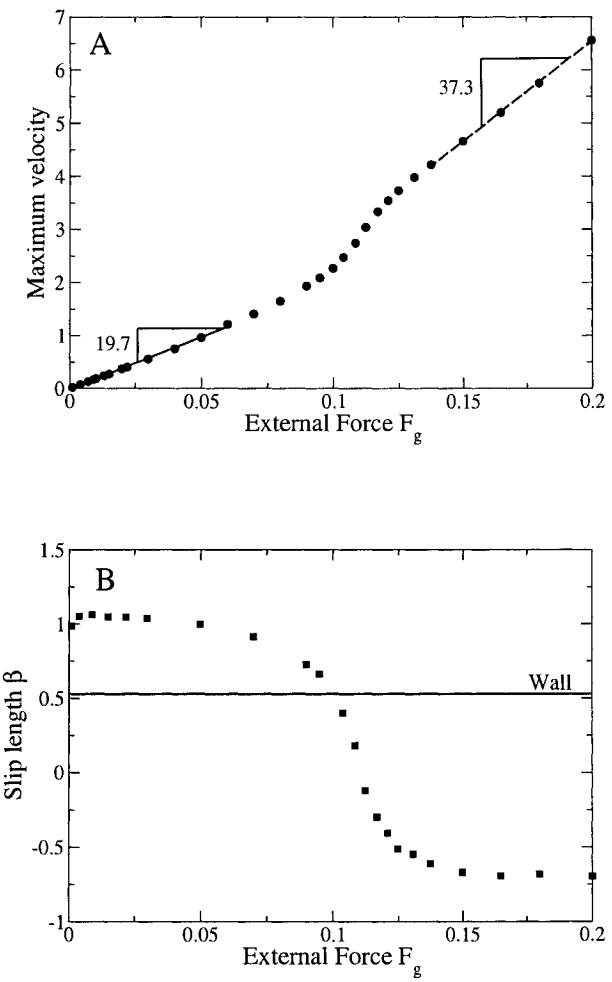

Fig. 3. *A) Mean flow velocity mid-way between the walls. The transition region found between $F_g = 0.1$ and $F_g = 0.125$ is the result of a dynamic transition from the noslip to the slip state. B) By fitting the flow pattern with a 6-th order polynomial, the z-position where the velocity of the solvent particles goes to zero can be extrapolated. The figure shows these extrapolated slip lengths as a function of the applied external force F_g. An inflection point is found at $F_g^* = 0.110(2)$. The horizontal line shows the mean position of the center of mass of the wall particles.*

To create a Poiseuille flow between the two solid planes, an external force in the x-direction is applied on each solvent particle [12]. This force can be likened to a gravitational force F_g which is fixed for the duration of a particuliar simulation. Of course, the addition of this force pumps energy into the system. This additional energy must be removed otherwise the temperature would rise and the walls would loose their structural integrity. In order to keep the system at a constant temperature, we divide the system in the z-direction into multiple layers and we rescale in each

of the layers the particles' peculiar velocities (velocities of particles with respect to the center of mass of the layer). The extra kinetic energy is then properly removed and the simulation produces a Poiseuille flow with the predicted parabolic velocity profile (see Fig. 2).

The relationship between the maximum fluid velocity $v_{\max}$ (found at the mid-point between the two walls) and the acceleration parameter F_g (in units of $\epsilon/\sigma_{\mathrm{LJ}}$) is shown in Figure 3A. By fitting the flow profile between the two walls with a polynomial (see the example shown in Fig. 2), one can find the slip length β (which is the point in space where the velocity becomes zero) via extrapolation (Fig. 3B). When the value of β corresponds to a position inside the wall, the solvent particles slip along the surface of the wall. A weak driving force gives a linear relation between $v_{\max}$ and F_g from $F_g = 0$ to about $F_g = 0.1$. Over that range, the value of β remains essentially constant (at about $\frac{1}{2}\sigma_{\mathrm{LJ}}$ above the row of wall particles) and clearly indicates a no-slip boundary condition at the wall [13–16]. A transition then occurs between $F_g = 0.1$ and $F_g = 0.125$ and the no-slip condition disappears. This transition can be best characterized by the inflection point $F_g^* = 0.110(2)$ (this provides a simple mathematical way to define the slip/no-slip transition from either the $v_{\max}$ vs. F_g curve or the β vs. F_g curve). For larger values of F_g, the solvent particles are slipping over the surface. The reduced friction at the wall then allows all solvent particles to globally increase their speed, including the ones in the middle region between the walls. This phenomenon is analogous to pulling a hard object along a rough surface. The solvent particles in contact with the wall are immobile in the no-slip regime because the driving force F_g is too low to overcome the forces of static friction. These stagnant solvent particles generate a strong frictional force on the next solvent layer which in turn slows down all solvent particles up to the middle point in the channel. Once the threshold for the maximum static frictional force is passed, the no-slip condition no longer applies. Slipping solvent particles have a smaller effect on the next layer, allowing the solvent velocity in the middle of the channel to increase. Friction still exists between the wall and the solvent particles, but instead of static friction, we now have kinetic friction; as a consequence, the slope of the $v_{\max}$ vs. F_g curve is higher than in the no-slip regime (Fig. 3A). In fact, we find a no-slip slope of $\frac{\delta v}{\delta F_g} = 19.7$ while we have $\frac{\delta v}{\delta F_g} = 37.3$ past the transition regime, which represents a doubling of the impact of the external force. In this article, all our simulations are made with a value of F_g between 0 and 0.1, in order to stay in the no-slip regime.

Equations (7)–(9) with F_g are used to calculate the force on each particle in the system at each time step. The equation of motion is then solved using a velocity Verlet algorithm [17]. A more complete description of our Molecular Dynamics method can be found in Refs. [18,19]. Other simulation methods have been used to study the current problem such as an hybrid method between Computational Fluid Dynamics (CFD) and MD [20], as well as a first-principle path integral Monte Carlo method [21].

4 Results

4.1 Chain extension

In this section we examine the relation between the mean chain extension and the Weissenberg number Wi. To calculate Wi, one needs to define and extract $\dot{\gamma}$ and τ_{relax} from the simulations. The shear rate $\dot{\gamma}$ is the change of velocity from a reference point to another point in space divided by the distance (perpendicular to the flow) between these two points. For simplicity, we characterize the parabolic flow profile by its mean slope between the z-position where the velocity is zero and the mean position of the last bead of the chain (see Fig. 2). This approximation takes into account only the section of the curve where the chain's probability of presence is non-negligible. As usual [5], the relaxation time was determined by fitting the time decay of the autocorrelation function of the chain end-to-end vector in the absence of a solvent flow (not shown). This gives the following relation [22]

$$\tau_{\mathrm{relax}} \simeq 3.51 \left(N - \frac{1}{2}\right)^{1.71}. \tag{10}$$

Equation (10) gives $\tau_{\mathrm{relax}} \simeq 564$, 1145 and 1883 for N =20, 30 and 40, respectively. We note that the exponent $1.71 = 3 \times 0.57$ of equation 10 is consistent with Zimm's prediction [6] of $3\nu \simeq 3 \times 0.588$. The contour length L was calculated as the sum of the distances between consecutive beads in the chain plus $\frac{1}{2}\sigma_{\mathrm{LJ}}$ for each end of the chain (this represents the additional space occupied by the end beads).

Figure 4 shows several ways to represent the effects of a shear flow on the chain end-to-end distance h_x for $N = 30$. The mean extension $\langle h_x \rangle$ of the polymer increases monotonically with the Weissenberg number Wi (Fig. 4A), and it eventually saturates for large values of Wi because the polymer then approaches its maximum extension $h_x = L$. As expected, the curve converges towards the mean equilibrium extension $\langle \mathbf{h} \cdot \hat{\mathbf{x}} \rangle = 0$ for small values of Wi.

As we can observe in Figure 4B, the standard deviation (SD) of h_x is very large for small Weissenberg numbers $Wi \leq 35$, but then decays for larger Wi's. The high-fluctuation region is thus an ideal place to look for the cyclic motion reported by Ladoux *et al.* [4]. Note that we did not explore the region $0 < Wi < 4$ because the simulation times required to obtain reliable results were too long with the available computing resources.

To explain the data in the weak stretching limit $\langle h_x \rangle \ll L$, one can naively use the Pincus blob theory [23] and the corresponding scaling law $\frac{h_x}{N} \sim f_x^{2/3}$, where $f_x \simeq R_g^2 \dot{\gamma} \eta$ is the friction force on the chain. Since the unperturbed radius of gyration R_g scales like $N^{3/5}$, one gets

$$\varepsilon = 1 - A \frac{Wi^{2/3}}{N^{2/5}} \tag{11}$$

where A is a constant. The Brochard-Wyart trumpet regime theory [24], which uses the Pincus blob theory more rig-

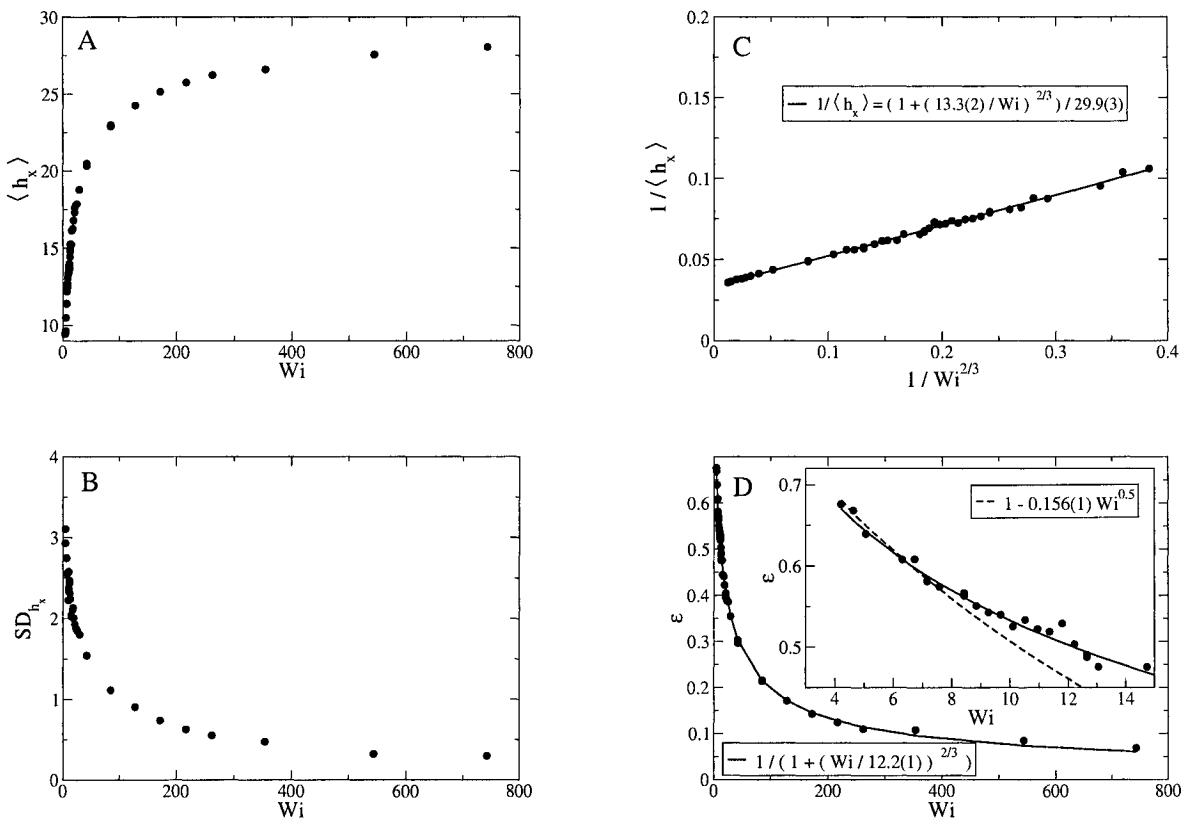

Fig. 4. *Various plots examining how the mean extension of a $N = 30$ polymer chain varies with the Weissenberg number Wi. A) The average extension in the x-direction increases monotonically with Wi. B) Standard-Deviation (SD) of h_x versus Wi. C) Plot of $1/\langle h_x \rangle$ vs. $1/Wi^{2/3}$; the data fall on a single straight line, as suggested by Eq. 15. D) Plot of the unstretched polymer fraction ε versus Wi with the fit proposed in equation (16). The inset shows both fits (Eqs. (12) and (16)) for $4 \leq Wi \leq 8$.*

orously, predicts

$$\varepsilon = 1 - B\frac{Wi^{1/2}}{N^{2/5}} \tag{12}$$

where B is a constant. This scaling law is predicted to be valid for $Wi = 1$ to 15. On the other hand, the large stretching limit $\varepsilon \ll 1$ can be obtained by rewritting equation (5) as

$$\varepsilon = C\frac{N^{1/5}}{Wi^{2/3}} \tag{13}$$

where C is a constant.

We now propose to find an approximate interpolation formula that could replace equations (11) and (13). First, we rewrite equation (13) as

$$\frac{\langle h_x \rangle}{L} = 1 - \frac{CN^{1/5}}{Wi^{2/3}} \simeq \frac{1}{1 + \frac{CN^{1/5}}{Wi^{2/3}}}, \quad Wi \gg 1. \tag{14}$$

Equation (14) indicates that a plot of $1/\langle h_x \rangle$ *vs.* $1/Wi^{2/3}$ should yield a straight line. Figure 4C shows the expected linear regime for large Wi, and surprisingly it shows the same linear regime for small Wi. This immediately suggests the following simple interpolation function

$$\frac{\langle h_x \rangle}{L} = \frac{1}{1 + \left(\frac{Wi^*}{Wi}\right)^{2/3}} \tag{15}$$

where $Wi^* \sim N^{3/10}$ is the critical Weissenberg number that separates the weak and strong stretching limits. The two-parameter fit in Figure 4C gives a critical value of $Wi^* \cong 13.3(2)$ as well as an effective contour length $L \cong 29.9(3)$, fully consistent with the expected contour length of our thirty-bead chain. Similarly, an interpolation equation for ε can be written as

$$\varepsilon = \frac{1}{1 + \left(\frac{Wi}{Wi^*}\right)^{2/3}} \tag{16}$$

Figure 4D shows that this is an excellent interpolation formula in this case too (the critical Weissenberg number is found to be $Wi^* \cong 12.2(1)$ using this slightly different, one-parameter fitting method).

Equation (16) gives the same result as the Ladoux equation (Eq. (13)) for large Wi and compares well with our simulations. For small Wi, equation (16) appears to describe our simulation data better then the original theory of Brochard-Wyart. Our interpolation formula gives for the small limit $\varepsilon \sim 1 - BWi^{2/3}$ (in agreement with the naive theory of Eq. (11)) while equation (12) shows a $Wi^{1/2}$ power law. As mentioned above, the Brochard-Wyart scaling law is expected to be valid for the range $Wi = 1$ to 15. We found that it fits our data well only up to $Wi = 8$. In fact, both equations (12) and (16) give a decent fit of our data (see inset in Fig. 4D) for $Wi < 8$. The Brochard-Wyart power law gives a slightly better fit than equation (16) over this restricted range, but the difference is not significant. One needs to take also into account the fact that the Standard-Deviation SD_{h_x} is quite high in the small extension regime. Thus the difference between both fits is negligible. We can only conclude that the Brochard-Wyart power law appears to work well for very small values of Wi, while our interpolation formula gives a good overall fit to our data.

Figures 5 and 6 illustrate that equations (15) and (16) also work well for $N = 20$ and 40 polymer chains. The scaling law $Wi^* \sim N^{3/10}$ is included in both graphs and brings all three sets of data together. The fit in both cases was made using all the data. We get a critical Weissenberg number $Wi^* = Wi_0 N^{3/10}$ where the prefactors $Wi_0 = 4.17(6)$ and 4.02(9) which are fully consistent with each other. We must stress the fact that the scaling law $Wi^* \sim N^{3/10}$ comes from the Ladoux and Doyle theory; therefore, it is not obvious why it works well even for small and moderate stretching. Since the difference between the scaling laws predicted by the different theories is rather small, one would perhaps need simulation data for much larger chains to clarify this point; this is currently beyond what is feasible with available computing power.

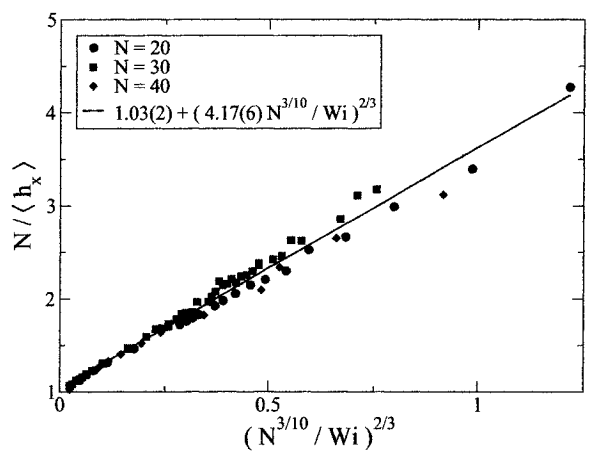

Fig. 5. *Plot of* $N/\langle h_x \rangle$ *vs.* $\left(N^{3/10}/Wi\right)^{2/3}$ *for various molecular sizes* N.

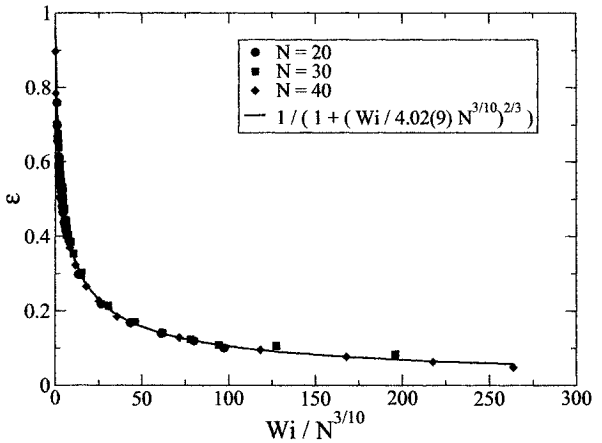

Fig. 6. *The unstretched fraction* ε *vs.* $Wi/N^{3/10}$ *for various molecular sizes* N.

4.2 Cyclic dynamics of the polymer

In order to study the possible existence of the cyclic motion described by Doyle *et al.* [1] which is in a way similar to the rotations motion of a tumbling "free" chain in a shear flow [25], we can examine the time evolution of the polymer's end-to-end distance $h_x(t)$ and the angle $\phi(t)$ between the wall and the vector joining the anchor point to the center of mass of the chain. Figure 4B indicates that this peculiar type of motion is more likely to exist for $Wi^* < Wi < 25 - 35$ in the case of our FJC. Figure 7 shows that although the variations of $h_x(t)$ and $\phi(t)$ tend to be of opposite signs, there is a fair amount of randomness. A four-step cycle is shown in Figure 7A, and the corresponding conformations are shown in Figure 7B. During the first step, the fluctuations of compact polymer conformations cause it to explore a region far away from the wall. Then the faster average flow at this position grabs the chain and extends it rapidly (the second step). At the end of the extension step, the polymer behaves like a lever and it is pushed back slowly to the wall by the flow (third step). When the polymer is close to the wall it retracts to a more compact state (fourth step) because the slower flow in that region cannot keep the polymer in an extended state. The polymer then "waits" for the next fluctuation to restart the cycle again. In effect, this is a periodic dynamical hysteresis cycle.

A straightforward quantitative way to look at the cyclic motion is to compute the normalized cross-correlation function $C(\tau)$ between $h_x(t)$ and $\phi(t)$ defined by

$$C(\tau) = \frac{\langle \phi(0) \times h_x(\tau) \rangle - \langle \phi \rangle \langle h_x \rangle}{SD_\phi \times SD_{h_x}} \qquad (17)$$

where $SD_A \equiv \sqrt{\langle A^2 \rangle - \langle A \rangle^2}$ is the standard-deviation of A. Schroeder *et al.* [26] used a similar cross-correlation

function for tumbling "free" sheared DNA molecules but Figure 8A shows a strong anti-correlation between $h_x(t+\tau)$ and $\phi(t)$ at equal time ($\tau = 0$); in other words, the chain tends to be in small h_x / large ϕ or large h_x / small ϕ conformations corresponding to conformations 1 and 3 of Figure 7B, respectively. Moreover, a positive cross-correlation maximum appears at $\tau > 0$ for shear rates in the range $Wi = 6.7$ to $Wi = 35.6$. Delayed positive cross-correlations correspond to the transitions from conformation 1 to conformation 3 or vice-versa (see Fig. 7B). The position τ_+ of the maximum is thus a direct measure of the average duration of the cycle.

A different point of view is provided by Figure 8B for a Weissenberg number $Wi = 17.3$ (which gives a characteristic time $\tau_+ = 288$). In this representation, we look at the average of $\phi(0)$ for a given value of $h_x(0+\tau)$ and several time delays τ. Note that the overall mean values of ϕ and h_x are given by the horizontal and vertical lines, respectively. At equal time (i.e., for $\tau = 0$), the curve is going from the second to the fourth quadrant, demonstrating that these two variables are indeed anti-correlated. When $\tau = \tau_+ \cong \frac{1}{5}\tau_{\text{relax}}$, however, the curve goes from the third to the first quadrant, i.e., the variables are correlated. For $\tau = 5\tau_+$, there is no correlation and the line is oscillating around the overall average value of ϕ.

Finally, Figure 9A and B show that τ_+ decreases like $Wi^{-2/3}$ (data shown for $N = 30$ and 40); an inverse dependence is expected since larger $\dot{\gamma}$ lead to faster chain stretching dynamics. We note that the power law is identical to the one predicted by equation (5). Furthermore, we find that $\tau_+ \sim N$. The normalized value $C(\tau_+)$ of the cross-correlation function at the critical time $\tau = \tau_+$ increases to reach a maximum value around $Wi \cong 20-35$ for $N = 30$ and 40 (Fig. 9C and D). This maximum indicates the best region to look for the cyclic motion. We also note that there is essentially no cyclic motion ($C(\tau_+) \cong 0$) for $Wi < Wi^*$, consistent with the fact that Wi^* corresponds to the shear rate where we observed the transition between small and large stretching (see section 4.1).

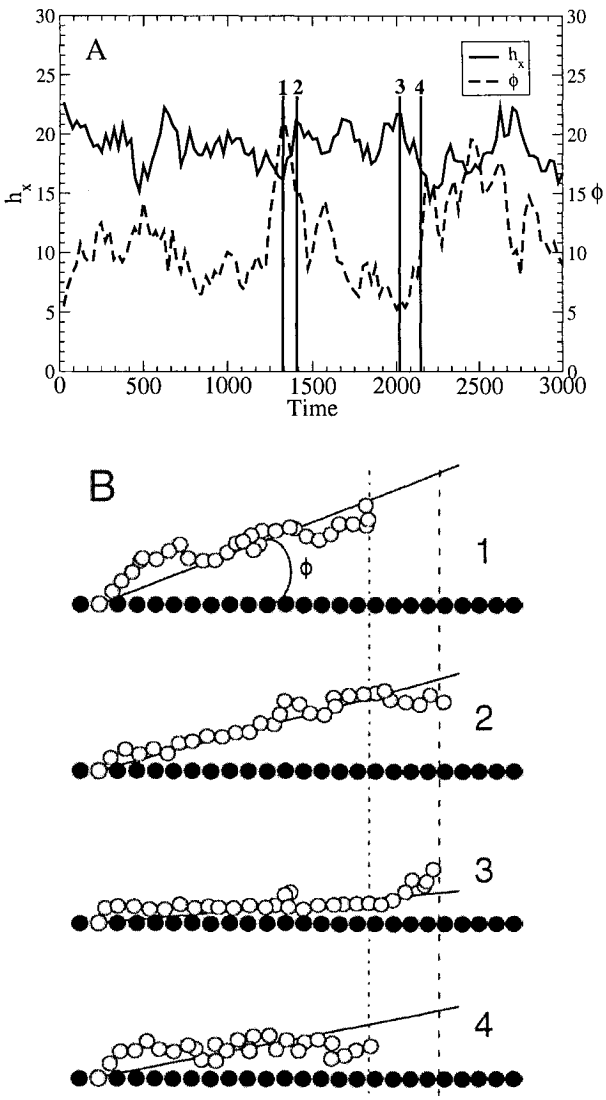

Fig. 7. *A) An example of cyclic polymer dynamics is described using the time evolution of the chain extension h_x and the angle ϕ for $N = 30$ and $Wi = 21$. B) Actual conformations of the chain at specific points in time. 1) The polymer is exploring the space away from the wall while being in a somewhat compact state. 2) The strong flow present far from the wall causes the chain to extend. 3) The extended polymer is pushed down slowly like a lever by the flow. 4) The chain returns to a more compact state because the flow velocity vanishes close to the wall.*

4.3 Packing effect

At a nanoscopic scale, liquids form well-defined layers near walls [27]. Since our walls are molecularly flat, a FJC polymer (whose persistence length is indeed comparable to the thickness of these liquid layers) will feel the effect of this local solvent packing, especially in the later phase of the cyclic motion (see conformation 3 of Fig. 7B). Looking at the chain extension h_z in the z direction, we see that the related distribution function shows some preferred positions near the wall that correspond to at least 3−4 clearly distinguishable liquid monolayers (see Fig. 10A). In the y direction, we also observe highly localized maxima near the wall (Fig. 10C), especially in the first liquid monolayer (Fig. 10B). As expected, the distance between the peaks in either direction is equal to the average intermolecular distance between the beads forming the walls ($\cong 1.05\sigma_{\text{LJ}}$).

The free end of the chain has preferred positions near the wall because the simple square lattice structure of the wall influences the local packing of the solvent molecules. Indeed, the particles (be they solvent molecules or monomers) close to the wall prefer to be intercalated between the beads of the wall. This creates a local packing effect which persists over a few monolayers away from the wall. In our simulation, there is no difference between the size of the monomers, the solvent particles or the wall beads; there-

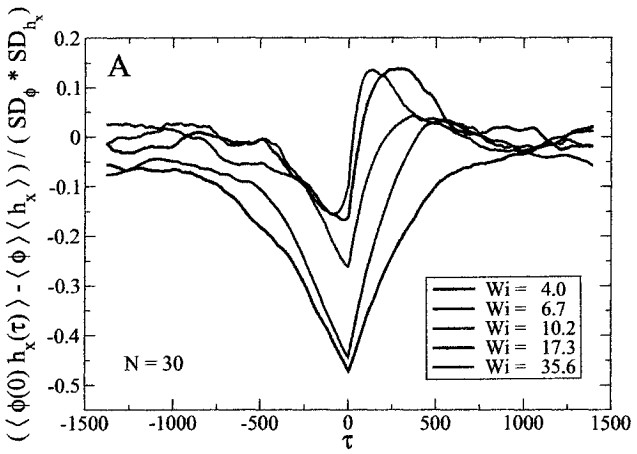

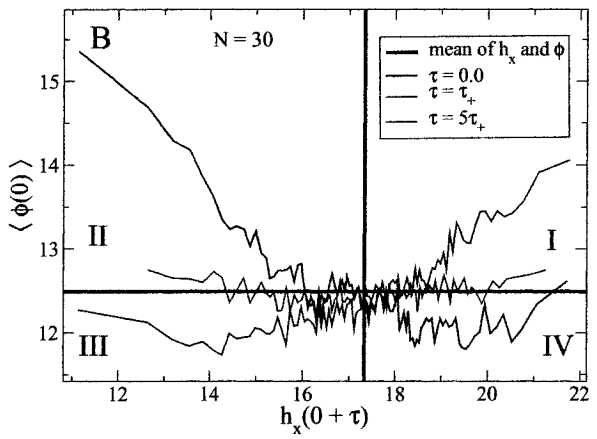

Fig. 8. *A) Cross-correlation between the chain extension h_x and the angle ϕ as a function of the time delay τ. Cross-correlation functions are shown for different values of the Weissenberg number Wi. The curves decay smoothly to zero for $\tau < 0$, while they reach a maximum before relaxing to zero for $\tau > 0$. At $\tau = 0$, the equal-time cross-correlation function is negative, indicating that h_x and ϕ are then anti-correlated. B) Conditional mean angular positions $\langle\phi(0|h_x(\tau))\rangle$ versus instantaneous extensions $h_x(\tau)$ for different values of the time delay τ for the case Wi = 17.3. The horizontal and vertical lines represent the global unconditional averages $\langle\phi\rangle$ and $\langle h_x\rangle$, respectively.*

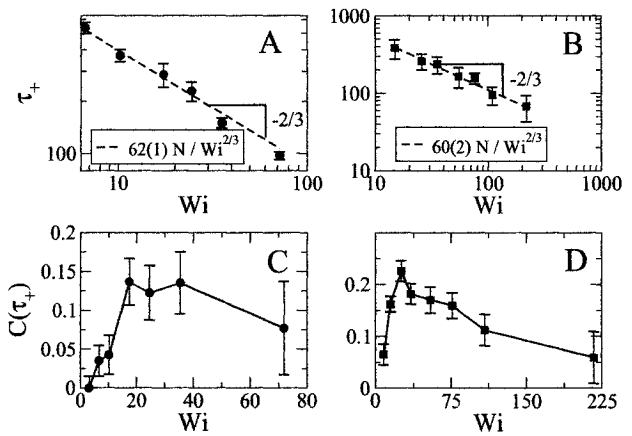

Fig. 9. *A) Critical delay time τ_+ for which the cross-correlation function reaches a maximum versus the Weissenberg number Wi for N = 30. B) Same as A) but for N = 40. C) Absolute value of the normalized cross-correlation for the critical time delay $\tau = \tau_+$ for N = 30. D) Same as C) but for N = 40.*

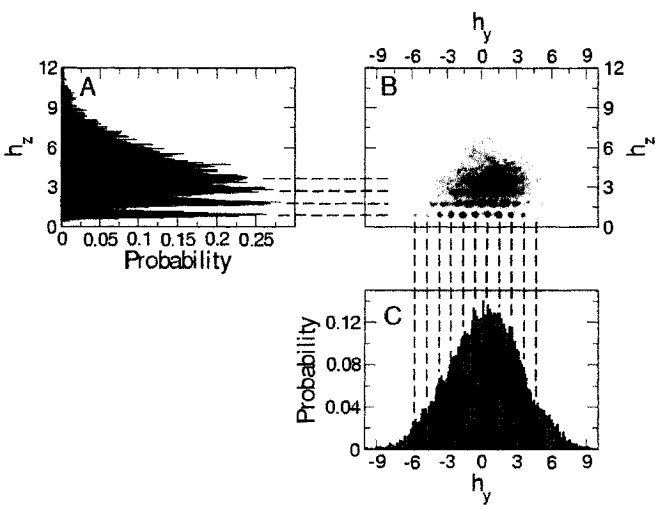

Fig. 10. *Probability distribution functions for the extension of a N=30 polymer chain tethered to a wall. The shear rate is Wi = 6.0. A) and C) show the probability distribution functions for the end to end distance in the z and y directions, respectively. B) Distribution of the instantaneous positions h_y and h_z of the end monomer of the polymer chain. The dotted lines point to the local maxima.*

fore, there is no size mismatch that could reduce the local packing of the beads. Adding the attractive part of the Lennard-Jones potential could increase packing effects even more. However, this nanoscopic effect is not likely to be very important in realistic systems because the walls are rarely molecularly flat; furthermore, polymers often have persistence lengths that exceeds the thickness of the solvent monolayers and monomers sizes that do not match the lattice spacing of the wall material.

4.4 Molecular Sticking Phenomenon

Our simulations also show evidence of another phenomenon that may occur in nanoscopic systems: molecular sticking. This phenomenon is actually related to the packing effects discussed in the section 4.3. Figure 11 shows that we

sometimes encounter situations where the polymer sticks on the surface of the wall for durations comparable to the equilibrium relaxation time τ_{relax}, (it would have completely relaxed during this period of time in absence of a flow). A similar nano-sticking phenomenon was observed previously by Drazer *et al.* [28] for a single sphere in a nanochannel. Note that there is no attractive interaction between the polymer and the walls in our simulations. Therefore, sticking must be attributed to entropic effects: by replacing solvent molecules near the wall, the polymer increases the entropy of the solvent. The solvent then pushes the polymer towards the wall, and the polymer tries to replace the solvent molecules in the first solvent monolayer. In order to escape from this flat conformation, polymer relaxation must start from the free end and propagate towards the fixed end, as shown at the bottom of Figure 11. Surface roughness would obviously interfere with the sticking phenomenon, and any residual effect would depend on the length scales (both vertical and in the plane) of the roughness. We are currently studying the case of a polymer in a poor solvent: one then expects important sticking effects triggered by the "hydrophobic" interaction.

4.5 Local Hydrodynamic Effects

Essentially all theories dealing with the effect of flows on polymer chains assume that the flow is not affected by the presence of the polymer; in other words, these theories are not self-consistent. This is the case with the theory of Ladoux and Doyle [4] and Brochard-Wyart [24]. The polymer does however affect the flow pattern: the velocity profile (and hence the local shear rate) of the solvent is changed by the presence of the polymer in the direction of the flow. As we can see in Figure 12, the flow surrounding the unattached end of the polymer slows down. The polymer acts like a shield against the flow. The fact that some solvent molecules are "trapped" by the polymer chain is consistent with the Zimm model of polymer hydrodynamics [19]. In Figures 12A and B, the length of the longest arrow represents 13% and 4% of the maximum velocity of the regular Poiseuille flow, respectively. Obviously, the local "effective" shear rate is affected. Figure 13 demonstrates the striking example of a simulation where the polymer reduces the local shear rate by $\cong$ 18%. Note that we did not take this into account when we plotted the x-axes in Figure 4.

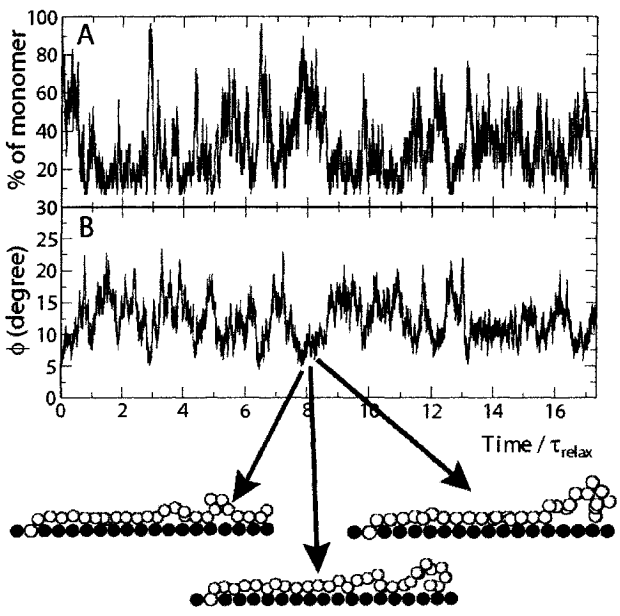

Fig. 11. *The polymer sticking phenomenon near the wall. A) Percentage of beads at a distance $z \leq \sigma_{\text{LJ}}$ from the wall as a function of time. B) Angular position ϕ of the chain's center of mass as a function of time. The three arrows point to actual conformations. The Weissenberg number was $Wi = 18.7$, the molecular size was $N = 30$, and the time axis is scaled by the equilibrium relaxation time $\tau_{\text{relax}} = 1145$.*

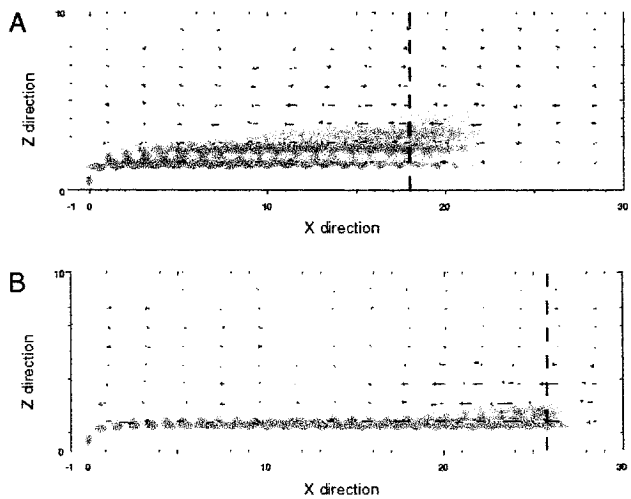

Fig. 12. *The vectors represent the difference between the actual flow and the expected flow in the x-z plane that includes the point where the polymer chain of molecular size $N = 30$ is attached. The shear rates are: A) $Wi = 35.6$ and B) $Wi = 184.7$. The length of the longest arrows represents 13% (A) and 4% (B) of the maximum velocity of the normal Poiseuille flow. The cloud of dots corresponds to the spatial distribution of the chain's beads (in a slice of width $\Delta y = 2\sigma_{\text{LJ}}$). The dotted line shows the position of the average end-to-end distance $\langle h_x \rangle$. A stronger shear flow keeps the chain closer to the wall and limits the impact of the polymer on the flow to a small region near the end of the chain.*

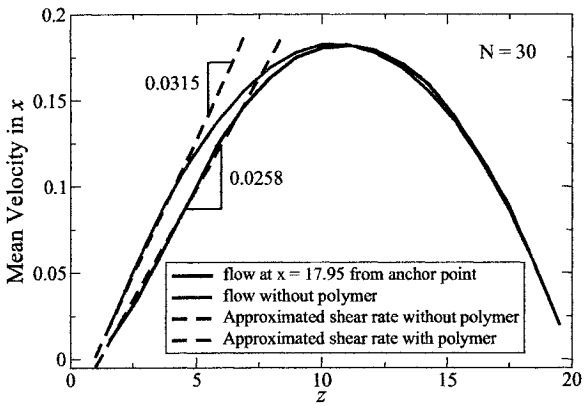

Fig. 13. *Flow profiles in the plane $y = 0$ and at position $x = 17.95$ (i.e., along the dashed lines in Fig. 12A), with and without the polymer attached to the wall. The presence of the polymer chain decreases the mean shear rate by about 18% in this case ($Wi = 35.6$).*

5 Conclusions

MD simulations allow us to obtain an accurate physical picture of the dynamics of a FJC attached to a wall and subjected to a shear flow. Although the motion of the polymer appears to be somewhat random at first sight, the extension-angle cross-correlation function $C(\tau)$ clearly demonstrates the presence of a net cyclic motion previously reported in ref. [1]. This peculiar motion was only observed for shear rates strong enough to lead to significant polymer stretching (e.g., when $Wi > Wi^* \cong 12.2(1)$ for $N = 30$). Furthermore, the amplitude of the cyclic motion decreased for higher shear rates (Wi larger than about 35 for $N = 30$) because SD_{h_x} decrease rapidly with Wi past this point (see Fig.4B).

Our MD results were compared with theory and it was found that the scaling law $\varepsilon \sim Wi^{-2/3}$ proposed by Ladoux and Doyle [4] for a FJC agrees with our MD data. Since the Pincus blob theory predicts a power law regime that contains a similar exponent in the weak-stretching limit, we proposed a new empirical formula (Eq. 16) for the dependence of ε upon Wi,

$$\varepsilon = \frac{1}{1 + \left(\frac{Wi}{Wi^*}\right)^{2/3}} \tag{18}$$

a formula that provides an interpolation between Ladoux's [4] regime (large Wi) and the Pincus regime. Our equation agrees nicely with the simulation data over the whole range of shear rates, and it thus provides a straightforward way to measure the critical Weissenberg number rate Wi^*.

It is interesting to note that the combination of Figure9A-B and equation (18) actually suggests the following formula:

$$\varepsilon = \frac{1}{1 + \frac{\tau_0}{\tau_+}} \tag{19}$$

where $\tau_+ \sim NWi^{-2/3}$ is the duration of the chain recirculation cycle and τ_0 is a critical time that is not predicted by the previous theories. To agree with equation (18) and the fact that $Wi^* \sim N^{3/10}$ in the Ladoux and Doyle regime, τ_0 needs to scale like $N^{4/5}$. For the systems studied in this article, we found that $\tau_0 = 23.7(1)N^{4/5}$ (data not shown). This critical time is much smaller than the equilibrium relaxation times τ_{relax} of our polymer chains. Equation (19) is in fact what one obtains when two processes, with durations τ_+ and τ_0, compete with each other. While τ_+ characterizes the effect of the shear forces that tend to stretch the polymer chains, τ_0 is not a function of the shear rate; it must therefore characterize the entropic forces competing against the shear flow. We thus simulated the nonequilibrium relaxation of a polymer chain tethered to the wall and initially stretched to almost full extension. After the free end is released (see Fig. 14), the compression of the end-to-end distance was found to follow the law $1 - h_x(t)/h_x(0) = (t/\tau_x)^{1/2}$, in agreement with the experimental results of Manneville *et al.* [29]. The relevant relaxation time τ_x was found to scale like $N^{4/5}$, exactly like the critical time τ_0. Therefore, equation (19) defines the competition between the shear forces and the entropic relaxation of a stretched polymer chain. Indeed, the nonequilibrium relaxation time τ_0 can be related to the fourth step in the cyclic motion of the chain: the chain is highly elongated and tries to relax along the wall.

Because our MD simulations are rather small systems, they are more typical of nanoscopic systems and some effects are unlikely to occur in most macroscopic systems. For instance, we showed that the end monomer of the chain tends to occupy positions that form a crystal structure near the wall, a consequence of the formation of well-defined solvent layers near a mildly corrugated wall. Similarly, we observed events where the chain appeared to stick to the wall for periods of time clearly exceeding the relevant equilibrium relaxation times.

A benefit of using MD simulations is the possibility to directly obtain the mean (and even instantaneous) flow profile everywhere in the system. This is most interesting in problems like this one because we must keep in mind that the polymer chain actually interacts self-consistently with the solvent flow (i.e., while the flow affects the chain conformations, the latter must also affect the flow), a fact that is often neglected in theories. Surprisingly, although we did observe a significant impact of the polymer on the magnitude of the flow near the wall, this did not seem to invalidate the power laws predicted by the theory.

The drawback of explicit MD simulations is the tremendous amount of CPU time required to compute all the interactions and displacements over a realistic and useful time interval. As CPU speeds increase, studying longer chains will become possible with reasonable simulation times.

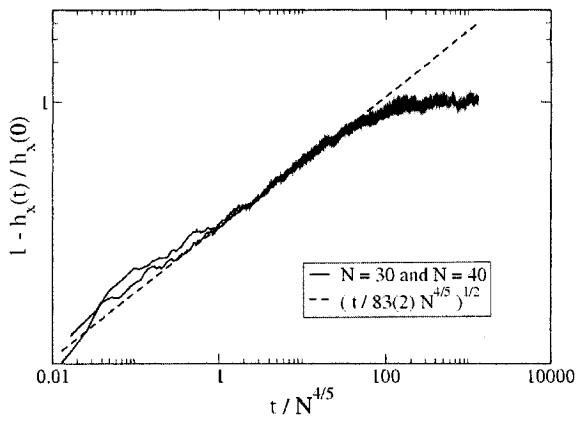

Fig. 14. *Plot of* $1 - h_x(t)/h_x(0)$ *vs.* $t/N^{4/5}$ *where* $h_x(0)$ *is the initial extension and* t *is the time. As long as* $0 < 1 - h_x/h_x(0) < 0.5$*, the chain relaxes following a* $t^{1/2}$ *power law [29,30]. Since the curves for* $N = 30$ *and* $N = 40$ *are superposed, the same type of line was chosen to represent both curves. Each curve is the average of ten distinct simulations with different initial conditions. Initially the end-to-end distance in the x-direction is fixed to* $(N-1)b$ *while the system equilibrates. Since one end of the chain is tethered to the wall it is stretched along the wall. Once the system is equilibrated, the constraint on the end-to-end distance is removed and the chain starts its relaxation process.*

In order to better model the DNA molecule studied in the experiments, we would need to use a Worm Like Chain (WLC). However, this would require substantially more computing power because one would then need larger chains to simulate molecules with a reasonable number of Kuhn lengths. Another problem of interest is the dynamics of systems with multiple tethered chains, with the goal to understand the effect of shear flows on the polymer chains forming a brush (and vice versa). In a future article, we will examine how the quality of the solvent affects the cyclic motion observed here for a FJC.

6 Acknowledgements

This work was supported by a Discovery Grant from the Natural Sciences and Engineering Research Council of Canada (NSERC) to GWS. YG would like to thank the Fonds Nature et Technologies (Québec) and the University of Ottawa for scholarships. This work used the computing resources of the High Performance Computing Virtual Laboratory (HPCVL) and of the Multimedia Advanced Computing Infrastructure (MACI). Finally, the authors would like to thank Martin Kenward for useful discussions and help with the programming.

References

1. P. S. Doyle, B. Ladoux, and J. L. Viovy *Phys. Rev. Lett.*, vol. 84, pp. 4769–4772, 2000.
2. J. Klein, Y. Kamiyama, H. Yoshizawa, J. N. Israelachvili, G. H. Fredrickson, P. Pincus, and L. J. Fetters *Macromolecules*, vol. 26, pp. 5552–5560, 1993.
3. P. Righetti and W. Hancock, eds., *Capillary Electrophoresis in Analytic Biotechnology.* New York: CRC Press, 1996.
4. B. Ladoux and P. S. Doyle *Europhys. Lett.*, vol. 52, pp. 511–517, 2000.
5. J. W. Hatfield and S. R. Quake *Phys. Rev. Lett.*, vol. 82, pp. 3548–3551, 1999.
6. I. Teraoka, *Polymer Solutions: An Introduction to Physical Properties.* New York: John Wiley & Sons, 2002.
7. J. F. Marko and E. D. Siggia *Macromolecules*, vol. 28, pp. 8759–8770, 1995.
8. A. Rahman *Phys. Rev.*, vol. 136, pp. 405–411, 1964.
9. L. Verlet *Phys. Rev.*, vol. 159, pp. 98–103, 1967.
10. R. C. Armstrong *J. Chem. Phys.*, vol. 60, pp. 724–728, 1974.
11. G. S. Grest and K. Kremer *Phys. Rev. A*, vol. 33, pp. 3628–3631, 1986.
12. J. Koplik, J. R. Banavar, and J. F. Willemsen *Phys. Rev. Lett.*, vol. 60, pp. 1282–1285, 1988.
13. J. L. Barrat and L. Bocquet *Phys. Rev. Lett.*, vol. 82, pp. 4671–4674, 1999.
14. M. Cieplak, J. Koplik, and J. R. Banavar *Phys. Rev. Lett.*, vol. 86, pp. 803–806, 2001.
15. C. Neto, V. S. J. Craig, and D. R. M. Williams *Eur. Phys. J. E*, vol. 12, pp. S71–S74, 2003.
16. P. A. Thompson and S. M. Troian *Nature*, vol. 389, pp. 360–362, 1997.
17. J. Gao and J. H. Weiner *Macromolecules*, vol. 29, pp. 6048–6055, 1996.
18. S. Barsky and G. W. Slater *Macromolecules*, vol. 32, pp. 6348–6358, 1999.
19. M. Kenward and G. W. Slater *European Physical Journal E*, vol. 14, pp. 55–65, 2004.
20. S. Barsky, R. Delgado-Buscalioni, and P. V. Coveney *J. Chem. Phys.*, vol. 121, pp. 2403–2411, 2004.
21. S. Yang, J. B. Witkoskie, and J. Cao *Chem. Phys. Lett.*, vol. 377, pp. 399–405, 2003.
22. S. Guillouzic and G. W. Slater *Phys. Rev. Lett.*, vol. (submitted for publication), 2004.
23. M. Rubinstein, *Polymer Physics.* Oxford University Press, 2003.
24. F. Brochard-Wyart *Europhys. Lett.*, vol. 23, pp. 105–111, 1993.
25. S. Liu, B. Ashok, and M. Muthukumar *Polymer*, vol. 45, pp. 1383–1389, 2004.
26. C. M. Schroeder, R. E. Teixeira, E. S. G. Shaqfeh, and S. Chu *Macromolecules*, vol. 38, pp. 1967–1978, 2005.
27. S. Iarlori, P. Carnevali, F. Ercolessi, and E. Tosatti *Surface Science*, vol. 211/212, pp. 55–60, 1989.
28. G. Drazer, J. Koplik, and A. Acrivos *Phys. Rev. Lett.*, vol. 89, 244501, 2002.
29. S. Manneville, P. Cluzel, J. L. Viovy, D. Chatenay, and F. Caron *Europhys. Lett.*, vol. 36, pp. 413–418, 1996.
30. Y. J. Sheng, P. Y. Lai, and H. K. Tsao *Phys. Rev. E*, vol. 56, pp. 1900–1909, 1997.

2.7 Technical note

Velocity rescaling done by layers could bring the reader to the conclusion that the dynamics presented in the manuscript are inaccurate. The reasoning could go as follow. Since the chain slows down the flow profile near the surface in the x-direction as seen in Figure 12, the average over the layer near the wall would be lower than expected. The rescaling done on the bead velocities would be more prominent than it should be, causing the flow velocity to give false information.

A simulation with velocity rescaling done only in the y and z-directions was used to verify this reasoning (see Fig. 2.1). One can see that both simulation curves with a chain present are superposed over the whole range of z. The superposition of the curves indicates that the dynamics obtained with rescaling in all directions are acceptable. The explanation must reside in the fact that the surface area covered by the chain is a small fraction of the total surface of the simulation system. The local change in flow profile caused by the polymer does not make a major difference in the total average flow in the x-direction of the whole layer.

To prevent any problem of the sort, the second manuscript implements rescaling in the y and z-directions only.

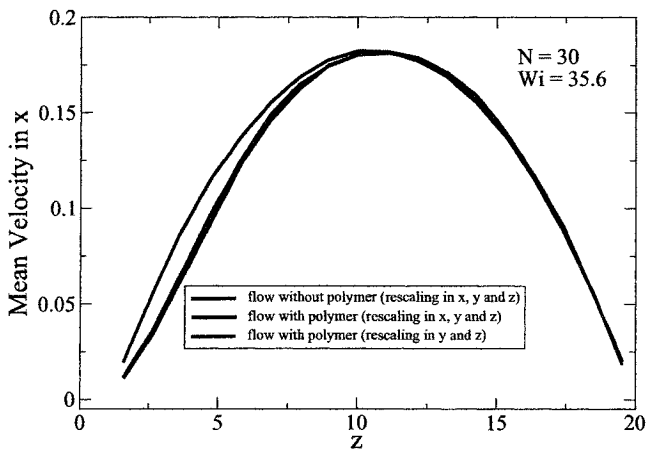

Figure 2.1: *Flow profiles in the plane $y = 0$ and at position $x = 17.95$, with rescaling in all three directions, with and without the polymer attached to the wall. The full line is the flow profile with a polymer but with no rescaling in the direction of the flow.*

Article II

Molecular Dynamics Study of Collapsed Tethered Polymers in Shear Flow.

Y. Gratton and G. W. Slater

To be submitted to European Physical Journal E.

2 Theory

Before looking at the different regimes investigated by Buguin and Brochard-Wyart for a collapsed FJC in a shear flow [7], we need to briefly review some basic concepts. We represent a collapsed chain by a collection of thermal blobs of size ξ, where ξ is also known as the correlation length. One blob contains g monomers of size b that follow a random path, thus giving $\xi = g^{1/2}b$. The aggregation of all the blobs gives a globule of radius r_c (see Fig. 1A). The relation between r_c and ξ is simply

$$r_c = \left(\frac{N}{g}\right)^{1/3} \xi \tag{1}$$

where N is the total number of monomers in the chain.

The parameter g is in fact a function of the temperature of the solvent [9]. Let $U(r)$ be the energy that is needed to bring a monomer from infinity to a distance r from another monomer. The Mayer f-function is the difference between the probability of finding both monomers at a distance r (the Boltzmann factor) and the case where $r = \infty$ [10],

$$f(r) = e^{\frac{-U(r)}{k_B T}} - 1 \tag{2}$$

where k_B is the Boltzmann constant and T is the temperature. The excluded volume v_e can conveniently be defined as the integral of the Mayer f-function from zero to infinity [10]:

$$v_e \equiv -\int_0^\infty f(r) d^3r. \tag{3}$$

A net repulsion between the two monomers corresponds to $v_e > 0$ while a net attraction corresponds to $v_e < 0$. Equation (3) can be divided into two parts: the first part ranges from $r = 0$ to $r = b$ while the second one goes from $r = b$ to $r = \infty$. If one uses hard-core repulsion for the first part, equation (2) is approximated as $f = -1$. The second part can be approximated by the series expansion $f(r) \cong -\frac{U(r)}{k_B T}$ if $|U(r)| < k_B T$. The excluded volume v can be estimated by including these approximations for both parts into equation (3) which gives

$$v_e \cong 4\pi \int_0^b r^2 dr - \frac{4\pi}{k_B T} \int_b^\infty U(r) r^2 dr. \tag{4}$$

Therefore, the integral can be approximated to

$$v_c \cong \frac{T - T_\theta}{T} a^3 \tag{5}$$

where $T_\theta \equiv -\frac{1}{b^3 k_B} \int_b^\infty U(r) r^2 dr$ is the temperature at which the chain acts like a ideal chain with a radius of gyration $R_\theta = bN^{1/2}$. When $T = T_\theta$, we have $v_e = 0$.

The competition between the effective repulsion between monomers and the corresponding entropy loss determines the conformation of the chain and can be described by the Flory theory [9] for the energy of one blob of size ξ. This approach assumes a uniform distribution of monomers inside the volume ξ^3. The free energy F_{Flory} that comes from the interaction between two monomers (with their respective excluded volume v_e) is

$$F_{\text{Flory}} \cong k_B T \times v_e \frac{g}{\xi^3} \times g. \tag{6}$$

The first term is the energy needed per exclusion. The second term is the probability of both monomers being in the same excluded volume for a given monomer (i.e., the probability of exclusion per monomer). The last term takes into account all the monomers in the blob. One could assume that $F_{\text{Flory}} \cong k_B T$ to get the number of monomers in one blob

$$g \cong \frac{b^6}{v_e^2}. \tag{7}$$

By substituting equation (5) in equation (7), we get the relation

$$g \cong \left(\frac{T}{T - T_\theta}\right)^2. \tag{8}$$

For temperatures above T_θ ($T > T_\theta$), the repulsion force wins over the entropy and the chain swells. In the region of $T \cong T_\theta$, the chain acts like an ideal chain. For temperatures lower than T_θ ($T < T_\theta$), a net attraction between monomers makes the chain collapse. This last region is the one of interest for this article.

We will now examine the three regimes for a collapsed FJC in a regular flow [7]: the small deformation regime, the stem and globule regime, and finally the ideal chain regime (see Fig. 1).

2.1 Small deformation : $\dot{\gamma} < \dot{\gamma}_1$

In the small deformation regime, the globule gets deformed by the shear flow $\dot{\gamma}$ but still stays as one slightly extended globule (see Fig. 1B). The surface energy F of this globule can be written as

$$F = \Pi \Delta A. \tag{9}$$

Here, Π ($= k_B T/\xi^2$) is the surface tension while the difference in surface area is $\Delta A \approx (s - r_c)^2$, where s is the chain span in the direction of the shear flow. The free energy thus gives the chain tension

$$f \cong \Pi (s - r_c). \tag{10}$$

Because we are in the small deformation regime, we can assume that the globule dimensions parallel and perpendicular to the wall are on the order of r_c which gives us a frictional force

$$f_v \cong \eta r_c^2 \dot{\gamma} \tag{11}$$

where η is the solvent viscosity. Given that the chain tension (10) equals the friction force (11), the chain span is equal to

$$s \cong \frac{\eta r_c^2 \dot{\gamma}}{\Pi} + r_c = \frac{\dot{\gamma}}{\dot{\gamma}_1} \xi + r_c. \tag{12}$$

The upper limit for this regime, $\dot{\gamma}_1$, is attained when the friction force becomes comparable to $k_B T/\xi$ (i.e., $\eta r_c^2 \dot{\gamma}_1 = \frac{k_B T}{\xi}$); this gives

$$\dot{\gamma}_1 = \frac{k_B T}{\eta r_c^2 \xi}. \tag{13}$$

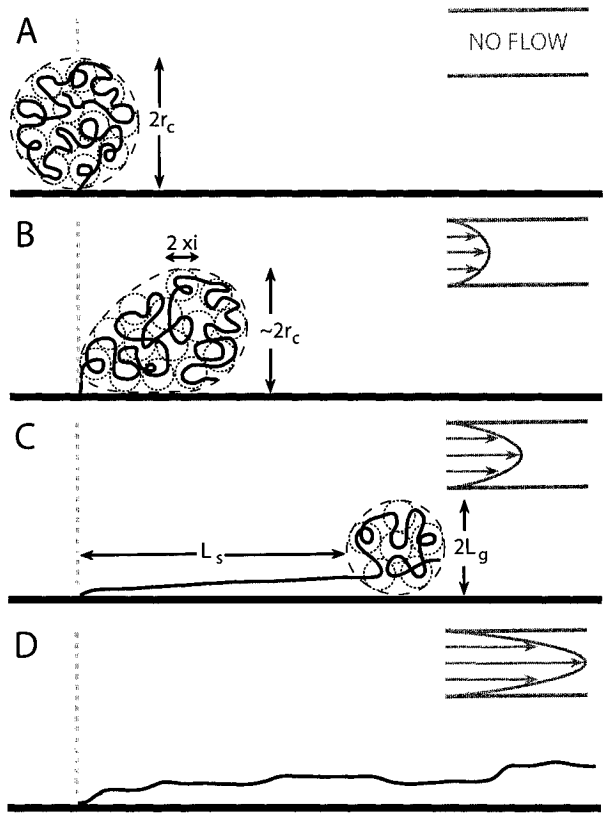

Fig. 1. *A schematic picture of the four conformations a collapsed chain can take. A) With no flow applied, the polymer collapses into a ball. The small dotted circles represent the blobs in the globule. B) A weak shear flow moves and deforms slightly the globule in the direction of the flow. C) An intermediate flow creates a stem conformation with a smaller globule at the end. D) A strong flow extends completely the chain to an almost straight line.*

Beyond this point, some blobs open up.

2.2 Stem and globule $\dot{\gamma}_1 < \dot{\gamma} < \dot{\gamma}_2$

We now model the chain with two sections. We have a globule containing n^* monomers at the free end of the chain, but the globule is now attached to the tethered point via a fully extended section of $N - n^*$ monomers called the "stem" (see Fig. 1C). The radius L_g of the globule is related to its number of monomers by

$$L_g = \left(\frac{n^*}{g}\right)^{1/3} \xi. \tag{14}$$

With the same logic that we used before, one can state that the tension in the chain at the meeting point between the stem and the globule is equal to both the friction on the globule and the Pincus elastic force, so that

$$\eta L_g^2 \dot{\gamma} = \frac{k_B T}{\xi}. \tag{15}$$

The stem section is considered a fully stretched ideal chain of height b (which is smaller than ξ) and length L_s. We approximate the length of the stem as

$$L_s \cong (N - 1 - n^*)b. \tag{16}$$

We have to point out that equation (16) is a simplified version of Buguin's theory [7]. The total chain span s is the addition of L_s and $2L_g$ which gives

$$s \cong (N - 1 - n^*)b + 2\left(\frac{n^*}{g}\right)^{1/3} \xi. \tag{17}$$

The combination of equations (13)–(15) gives us $n^* = N\,(\dot{\gamma}_1/\dot{\gamma})^{3/2}$ which can be used in equation (17) to obtain the new relation

$$s \cong Nb\left[1 - \left(\frac{\dot{\gamma}_1}{\dot{\gamma}}\right)^{3/2}\right] + 2\left(\frac{\dot{\gamma}_1}{\dot{\gamma}}\right)^{1/2} r_c - b. \tag{18}$$

This regime ends at a critical shear rate $\dot{\gamma}_2$ where the globule size is reduced to ξ. The relation $\eta\xi^2\dot{\gamma}_2 = \frac{k_B T}{\xi}$ gives

$$\dot{\gamma}_2 = \frac{k_B T}{\eta \xi^3} = \frac{r_c}{\xi}\dot{\gamma}_1. \tag{19}$$

2.3 Ideal chain $\dot{\gamma} > \dot{\gamma}_2$

Beyond the flower-globule, the chain is reduced to the stem from the previous regime: an ideal chain completely extended in the flow direction (see Fig. 1D). Indeed, for large $\dot{\gamma}$, the term $\dot{\gamma}_1/\dot{\gamma}$ in equation (18) tends toward 0 and we get

$$s \cong (N - 1)\, b. \tag{20}$$

In this regime the chain is always pushed by the shear flow flat against the wall in a fully extended state. The large shear rate prevents all relaxation by the chain.

3 Molecular Dynamics Model

We begin by briefly describing the system. It is enclosed between two walls made of a single sheet of beads. The volume between the walls is filled with solvent particles represented by united-atom beads. These solvent beads surround the polymer which is attached by one end to the middle of a wall. All beads mentioned above interact via the same general form of the shifted Lennard-Jones potential [11,12]

$$\begin{aligned} U_{\mathrm{LJ}}(r_{ij}) &= 4\epsilon\left[\left(\frac{\sigma_{\mathrm{LJ}}}{r_{ij}}\right)^{12} - \left(\frac{\sigma_{\mathrm{LJ}}}{r_{\mathrm{cut}}}\right)^{12} - \left(\frac{\sigma_{\mathrm{LJ}}}{r_{ij}}\right)^{6} + \left(\frac{\sigma_{\mathrm{LJ}}}{r_{\mathrm{cut}}}\right)^{6}\right]; \quad r_{ij} < r_{\mathrm{cut}} \\ &= 0; \qquad\qquad r_{ij} \geq r_{\mathrm{cut}} \end{aligned} \tag{21}$$

where r_{ij} is the distance between the centers of beads i and j. The energy ϵ as well as the characteristic distance σ_{LJ} are set to 1 (in other words, they define the energy and

length scales, repectively), and the cutoff is $r_{\rm cut} = 2.5\sigma_{\rm LJ}$. The different interactions are included in the ϵ variable. For polymer-polymer interactions $\epsilon_{pp} = 1.5$, 3.0 or 4.0, while for all other interactions (polymer-wall, polymer-solvent, solvent-solvent, solvent-wall, wall-wall) $\epsilon_{xx} = 1.0$. The difference in ϵ for the different interactions allows the polymer to collapse to varying degrees (depending on the value of $\Delta\epsilon = \frac{1}{2}(\epsilon_{xx} + \epsilon_{pp}) - \epsilon_{xp}$).

A Finitely Extensible Nonlinear Elastic (FENE) potential links together consecutive monomers along the polymer chain [13,14]

$$U_{\rm FENE} = -\frac{1}{2}kR_0^2 \log\left(1 - \frac{r_{ij}^2}{R_0^2}\right), \qquad r_{ij} < R_0 \qquad (22)$$

where $k = 30\epsilon/\sigma_{\rm LJ}^2$ and $R_0 = 1.5\sigma_{\rm LJ}$. The wall beads are anchored using a harmonic potential of the form

$$U_w = \frac{1}{2}k_w {r_w}^2 \qquad (23)$$

where $k_w = 120\epsilon/\sigma_{\rm LJ}^2$ and r_w is the distance between the reference position for a bead (its mean position on a lattice structure) and its actual position. The standard MD units of length $\sigma_{\rm LJ}$ and time $\tau_{\rm LJ} = \sigma_{\rm LJ}\sqrt{m/\epsilon}$, where m is the mass, are used throughout this article.

The dimensions of the simulation box are $2.5N\sigma_{\rm LJ} \times 20\sigma_{\rm LJ} \times 20\sigma_{\rm LJ}$ in the x, y, and z-directions respectively. The number of beads in the polymer chain (N) is 20, 30 or 40. The tethering of the chain is produced by replacing a bead of the wall by one end bead of the polymer. Periodic boundary conditions exist in the x and y-directions while in the z-direction, the two walls take care of keeping the solvent in place (see Fig. 2).

The last condition needed in our system is a Poiseuille flow between the two walls. It is created by adding an exteral force in the x-direction on all the solvent beads [15]. The external force F_g (in units of $\epsilon/\sigma_{\rm LJ}$) acts like a gravitational force which is present at every simulation step. Extra energy is then pumped into the system. With no action taken, the system would not be able to prevent solvent particles from penetrating the walls and leaking. This temperature problem is taken care of via a rescaling of the fluctuations of the particles' velocities. One must divide the system into multiple layers in the z-direction and then rescale separately into each layer. The extra energy is removed and the temperature is stabilized. The division by layers is essential because the average velocity changes while moving from one wall to the other. The velocity profile one gets with the gravitational force is the expected parabolic Poiseuille flow [15].

Equations (21) - (23) with F_g represent all the forces present in the system. At each time step, the sum of all the applicable forces is calculated for each bead in the system. A velocity Verlet algorithm [16] calculates the next positions and velocities of all the beads. A detailed description of our MD method can be found in Refs. [17,18].

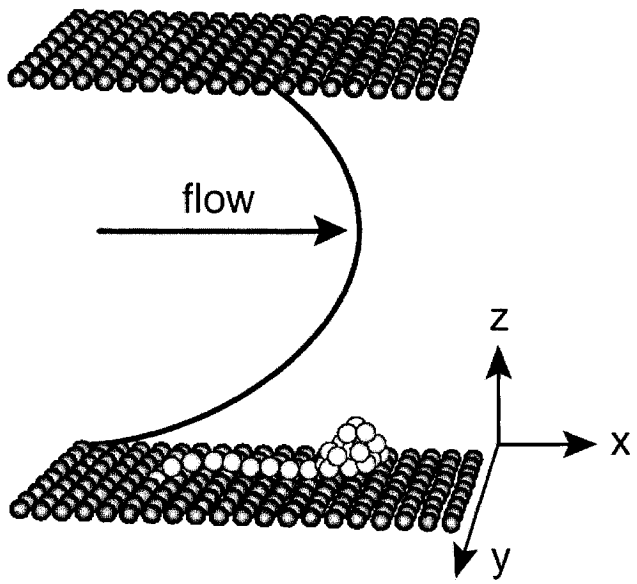

Fig. 2. *A schematic picture of the system investigated in this article. The collapsed FJC polymer chain is attached to the bottom wall and stretches out in response to the strong shear flow.*

4 Results

4.1 Chain extension

In this section we examine the relation between the chain span s and the shear rate $\dot{\gamma}$. The chain span s is defined as the absolute value of the difference in x-position between the two beads which are the farthest away from each other. The shear rate is the difference in velocity between two points in space divided by the distance between them. The distance needed is the one perpendicular to the flow between these points. We approximate the parabolic (Poiseuille) flow profile by its mean slope between the wall and the mean span in the z-direction when no flow is applied, a reasonable assumption since the chain is collapsed.

The effect of the shear flow on the mean chain span $\langle s \rangle$ is shown in Figure 3 for different values of ϵ_{pp} with $N = 30$. For $\epsilon_{pp} = 1.5$, the chain is in a transition state: the shape of the curve is similar to that obtained with a good solvent [19]. The chain is never fully collapsed and its extension increases monotonically with the shear rate. Doubling ϵ_{pp} to 3.0 collapses the chain into a globule for small shear rates (0 to $\sim$ 0.02). The chain then extends rapidly from around 10% to 75% of its full span with a small increase in shear rate ($\Delta\dot{\gamma} \sim 0.08$). Finally, for $\dot{\gamma} > 0.1$, the chain span slowly increases towards its maximum value. For $\epsilon_{pp} = 4.0$, the span curve follows the same qualitative regimes as in the $\epsilon_{pp} = 3.0$ case. The quantitative differences lie in where the transitions happen: the globule regime survives until $\dot{\gamma} \sim 0.05$, while a 75% span is reached only at $\dot{\gamma} \sim 0.12$. It is understandable that the chain remains in the globular regime longer since the net attraction between chain monomers are stronger. Hence,

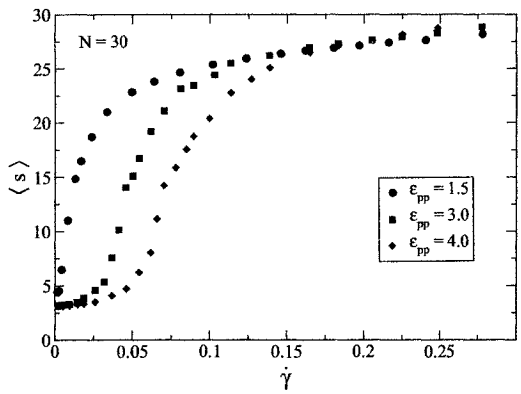

Fig. 3. *Plot of the mean conformation span* $\langle s \rangle$ *vs. the shear rate* $\dot{\gamma}$ *for three different values of the polymer-polymer interaction energy* ϵ_{pp}.

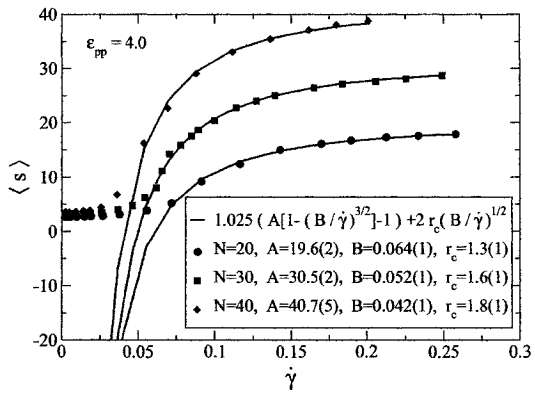

Fig. 4. *Plot of* $\langle s \rangle$ *versus* $\dot{\gamma}$ *for* $N = 20$, *30 and 40. The solid lines are fits using equation (18) with two parameters (A and B) for each N. The respective values for the parameters are shown for each N. The globule radius* r_c *is fixed.*

the last regime begins at a higher shear rate compared to the $\epsilon_{pp} = 3.0$ curve. One can also observe that, for large shear rates, the curves do not seem to tend toward the same maximum span (actually, the curves cross each other). This anomaly comes from the increase in average bond length b with higher ϵ_{pp}. In fact for $\epsilon_{pp} = 1.5$, 3.0 and 4.0, the average bond length b is respectively 0.985(1), 1.014(1) and 1.025(1) for $\dot{\gamma} = 0$. Since the well in the LJ potential gets deeper when increasing ϵ_{pp}, the total potential function (LJ + FENE potentials) for adjacent monomers favours conformations close to the minimum in the LJ potential (i.e., $2^{1/6} = 1.1225$).

Figure 4 shows the effect of $\dot{\gamma}$ on the mean span $\langle s \rangle$ for different values of N. We first focus on the *stem and globule* regime. The following version of equation (18) is used to fit all three curves with three parameters (A, B and r_c):

$$\langle s \rangle = \left(A \left[1 - \left(\frac{B}{\dot{\gamma}} \right)^{3/2} \right] - 1 \right) b + 2 r_c \left(\frac{B}{\dot{\gamma}} \right)^{1/2} ; \quad \dot{\gamma} > \dot{\gamma}_1, \tag{24}$$

where A corresponds to N and B to $\dot{\gamma}_1$. As one can see in Figure 4, the fits agree nicely with the simulation data. Also, they give us the expected values for A as well as the lower bound $\dot{\gamma}_1$ where we started the curve fitting. An enlarged view for small $\dot{\gamma}$ is shown in Figure 5; it provides us with a clearer view of the small deformation regime. Using equation (12) as a template with two parameters (B and C), we then get

$$\langle s \rangle = \frac{\dot{\gamma}}{B} \xi + C r_c ; \quad \dot{\gamma} < \dot{\gamma}_1, \tag{25}$$

where C is a prefactor of order unity. The values for $\dot{\gamma}_1$ are (within statistical errors) the same as the ones found previously in Figure 4. Also, the prefactor C is almost equal to 2 which makes sense since at $\dot{\gamma} = 0$, h should be equal to $2r_c$. The ideal chain regime can be verified with

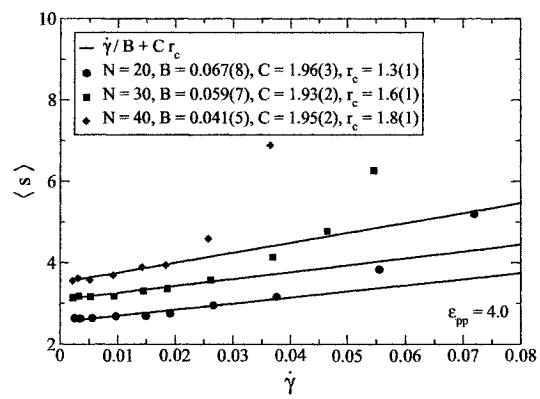

Fig. 5. *Plot of* $\langle s \rangle$ *versus small* $\dot{\gamma}$ *for* $N = 20$, *30 and 40. The fits where made with two parameters (B and C) for each N while the globule radius* r_c *was fixed to their respective values.*

Figure 4. All three curves tend toward their respective fully extended values $(N - 1)\, b$. We can only conclude that the model presented in this article works for the molecular lengths tested here.

4.2 Polymer dynamics

The presence of cyclic motion has been demonstrated by Gratton and Slater [19] via MD simulations for the repulsive and good solvent corresponding to $\epsilon_{pp} = 1.0$ and $r_{\text{cut}} = 2^{1/6}\sigma_{\text{LJ}}$. This behavior, first studied by Doyle *et al.* [1,8], was found in the region where the standard-deviation (σ) of the chain's end-to-end distance was very large. Figure 6 provides us with a similar view: the standard-deviation $\sigma(s)$ of the span s versus the shear rate $\dot{\gamma}$. We

observe quite a large increase in $\sigma(s)$ in the region $0.7 < \dot{\gamma} < 1.0$. Outside this region, all three data sets are indistinguishable. For the small shear rate region the superposition arises from the fact that the beads on the surface of the globule are the only ones able to interact with the solvent particles. The chain beads in the core of the globule cannot fluctuate as much. Since only the surface beads fluctuate, the standard-deviation is essentially independent of N. For shear rates larger than about 1.0, all three chain lengths only have 10 or less beads left in the globule which gives roughly the same $\sigma(s)$. On the other hand, the middle region shows differences between the three curves. This is due to the fact that the *stem and globule* regime starts at different shear rates for different molecular sizes N (see Fig. 4). The larger the number of monomers in the chain the earlier the *stem and globule* regime starts, which can be explained by the fact that, for larger N, the corresponding globule will feel more friction since it is higher in the shear flow.

If we are to find cyclic motions with the present system, it should be in the region where the fluctuations (and hence $\sigma(s)$) are maximum. The normalized cross-

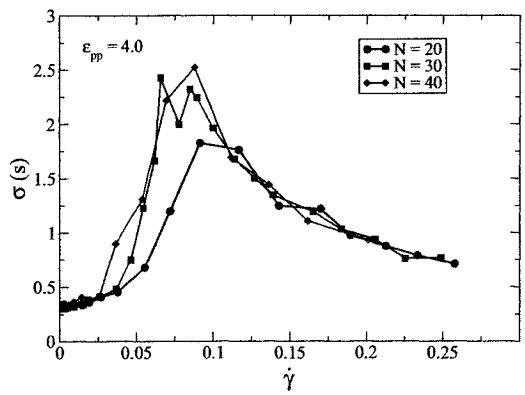

Fig. 6. *The standard-deviation (σ) of the span s reaches a maximum in the region* $0.7 < \dot{\gamma} < 1.0$.

correlation function $C_{h\phi}(\tau)$ between the end-to-end distance h in the direction of the flow and the angle $\phi(t)$ between the wall and the vector joining the anchor point to the center of mass of the chain gave Gratton and Slater [19] an indication of the presence of the cyclic motion for a good solvent. For our system, the relevant normalized cross-correlation function $C(\tau)$ is between $h(t)$ and $\phi(t)$ and is defined as

$$C_{h\phi}(\tau) = \frac{\langle \phi(0) \times h(\tau) \rangle - \langle \phi \rangle \langle h \rangle}{\sigma(\phi) \times \sigma(h)} \qquad (26)$$

where $\sigma(A) \equiv \sqrt{\langle A^2 \rangle - \langle A \rangle^2}$ is the standard-deviation of property A. The four-step cyclic motion found in Ref. [1] was not observed (not shown). A visual inspection of the actual chain movements (with the aid of an in-house visual software) shows why the cross-correlation function does not suggest the presence of cyclic motion. The globular section of the chain in the *stem and globule* regime is always pushed down like a lever by the higher velocities felt at the top of the globule. Since the other chain end is attached to the wall and the globule is pushed against the wall by the flow, ϕ stays constant, preventing all possibilities of a cyclic motion.

A normalized autocorrelation function for the span $s(t)$ ($C_{ss}(\tau)$) can give us some information about the dynamics of the chain in the *stem and globule* regime. The autocorrelation time τ_e, which is defined by the relation $C_{ss}(\tau_e) = 1/e \sim 0.368$, increases to a maximum around the same region in shear rate as the $\sigma(s)$ does (compare Fig. 7 to Fig. 6).

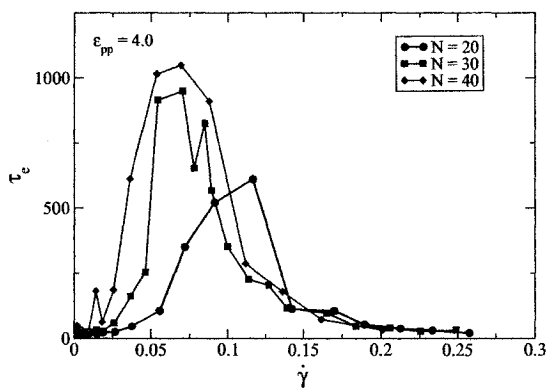

Fig. 7. *The autocorrelation time τ_e of the chain span s versus the shear rate $\dot{\gamma}$ for molecular sizes $N = 20$, 30 and 40.*

Another property of the dynamics of the chain in the $\dot{\gamma}$-region where $\sigma(s)$ and τ_e are maximum can be investigated via the probability distribution function for the span s. Figure 8 shows an interesting phenomenon: when $\sigma(s)$ is around its maximum, peaks at regular intervals appear in the probability distribution functions. For $\dot{\gamma} = 0.062$ and 0.078, peaks are spaced by the value of the bond length b. We can assume that, in the beginning of the *stem and globule* regime, the release and subsequent cannibalization of beads is a discrete process. With local fluctuations in the case where the globule is pushed away from the tethered point, a bead will leave the globule to become a part of the stem, adding by the way an extra b length to the total span of the chain.

The number of peaks per distribution in Figure 8 explains the span standard-deviation values found in Figure 6. The five peaks at $\dot{\gamma} = 0.062$ gives $\sigma \cong 2.5$, while four peaks at $\dot{\gamma} = 0.078$ gives $\sigma \cong 2.0$. We then see a transition with no clear peaks at $\dot{\gamma} = 0.114$, followed by the return of three peaks ($\sigma \cong 1$) at $\dot{\gamma} = 0.249$.

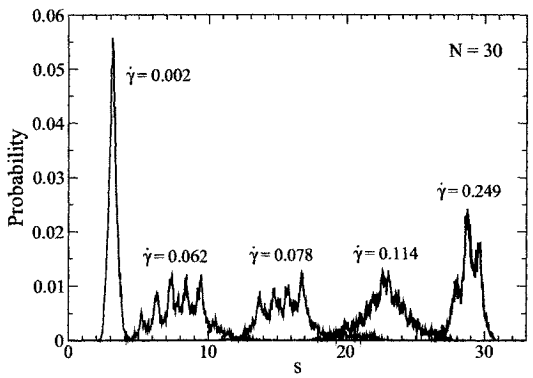

Fig. 8. *Probability distribution functions of the span s for different values of* $\dot{\gamma}$.

4.3 Dynamics for time-varying flows

Until now in this article, every simulation had a constant external force (like a gravitational force) fixed for the whole duration of the simulation. In this section, we will address the problem of an external force which changes linearly in time. The simulations now consist of three distinct sections. The first section is the equilibration time where no external force is applied and the chain collapses into a globule. Then the time counter is reset to zero and the external force is increased linearly in a way that will bring the system to a maximum F_g of 0.1 in half of the chosen total time. For the last section (the second half of the total time), the external force follows the reverse path, going from 0.1 back to 0.0. The external force is increased such that the system is in a quasistatic shear rate at all times. Figures 9A–C show the average span s of 20 distinct simulations for 3 different total ramping times t_T: 7500, 12500 and 25000. The presence of a large hysteresis in the force-extension curve can be explained by the following two facts. First, it is hard to open up a globule because its friction is small. This fact is supported by Figure 9 in which during the flow increase time (see arrow labeled 1) the chain stays in a globular form (small span s) for a long time before going to the *stem and globule* regime. Second, it is relatively easier to keep a chain in a stem-globule conformation because the stem section generates a large drag force as seen in the decreasing flow time period (arrow labeled 2) in Figure 9. The chain which starts in a fully extended conformation slowly reforms a globule at its tail, which makes the chain span decrease at a slower rate than during the first half of the simulation time. Thus, combining both facts with a finite t_T, a hysteritic behavior appears.

A semi-quantitative approach can be used to give more insights on this behavior. The frictional force on a ball (f_b) goes like

$$f_b \cong v_b \times 6\pi\eta R_h \cong \dot{\gamma} \times 6\pi\eta \left(n^*\right)^{2/3} b^2 \qquad (27)$$

where R_h is the hydrodynamic radius which is proportional to $(n^*)^{1/3} b$, and the velocity v_b is equal to R_h times the shear rate ($\dot{\gamma}$). On the other hand, the frictional force on a rod (f_r) aligned in the direction of the flow is

$$f_r \cong v_r \times 2\pi\eta L_s \cong \dot{\gamma} \times 2\pi\eta \left(N - 1 - n^*\right) b^2 \qquad (28)$$

where the velocity $v_r \cong b\dot{\gamma}$. The total drag force (f_f) is then

$$f_f \cong f_r + f_b \cong \dot{\gamma}\eta b^2 \left[2\pi \left(N - 1 - n^*\right) + 6\pi \left(n^*\right)^{2/3}\right]. \qquad (29)$$

It is possible for two chain spans found at different shear rates to feel the same total drag force. Let's choose our first chain span s_1 at $\dot{\gamma}_1 = 0.12$ on the increasing flow curve (see Fig. 10). Its total drag force f_1 can be calculated using equations (17) and (29)

$$f_1 \cong \eta b^2 \dot{\gamma}_1 \left[2\pi \left(N - 1 - n_1^*(s_1)\right) + 6\pi \left(n_1^*(s_1)\right)^{2/3}\right]. \qquad (30)$$

A second set of span and shear rates (s_2 and $\dot{\gamma}_2$) from the decreasing flow curve which feels a total drag force f_2 equal to f_1 can be calculated as follows:

$$\dot{\gamma}_2 \left[2\pi \left(N - 1 - n_2^*(s_2)\right) + 6\pi \left(n_2^*(s_2)\right)^{2/3}\right] = \dot{\gamma}_1 \left[2\pi \left(N - 1 - n_1^*(s_1)\right) + 6\pi \left(n_1^*(s_1)\right)^{2/3}\right]. \qquad (31)$$

The right-hand side of equation (31) is a known number; therefore, we are left with the function $\dot{\gamma}_2(s_2)$ since N is fixed. A fit of the decreasing flow curve of Figure 10 provides the extra equation to solve equation (31) for s_2 and $\dot{\gamma}_2$. We now end up with two different chain spans feeling the same total friction force. As one can see in Figure 10 the four sets of black-white dots show some examples of the previous calculation. The major difference in shear rates between related dots is a result of the fact that the friction coefficient of a rod aligned in the direction of the flow will always be greater than the friction coefficient of a ball (or globule). Hence, a given shear rate can provide two different chain conformations.

Figure 11 illustrates the trend which occurs when the total time t_T increases. An infinite ramping time t_T would bring the span trajectory on top of the dotted curve which corresponds to the case where F_g is unchanged for the whole duration of the simulation. This remarkable behavior shows that time-dependent phenomena (such as AC flows) can be highly non-trivial.

5 Conclusions

The results generated by our MD simulations shed light on the problem of collapsed tethered polymers in shear flow. A fascinating case of hysteresis which occurs when the shear flow strength changes linearly in time was reported. It shows the major difference between the friction coefficient of a rod aligned in the direction of the flow and of a globule, which allows two very different chain spans

to coexist at the same shear rate. Of course, since longer chain spans are less stable than smaller ones, they would eventually collapse to the smaller span if we were to use much slower ramps.

The simplified model used to describe the different regimes that the chain goes through for different shear rates agrees with our MD data. Equations (12), (18) and (20) can be successfully used as scaling laws to explain the chain span in respectively the *small deformation* regime, the *stem and globule* regime and the *ideal chain* regime.

In the *stem and globule* regime, large fluctuations were observed for the chain span in the direction of the flow. We did not observe the presence of cyclic motion as in the good solvent case [19]. The globule is the key to the absence of the cyclic motion: since the top part of the globule is exposed to higher shear rates, a lever force is pushing it towards the wall at all times. The chain must leave the proximity of the wall in order to start the cyclic motion and get extended by stronger flows. Since the first step of the cycle is always prevented, the chain never begins the cyclic motion. The main contribution of the span fluctuations comes from the competition between the globule and the stem. Depending on the local fluctuations of the solvent particles, the globule will either gain a monomer from the stem or give one back. At $\dot{\gamma} \sim 0.06$, up to five monomers are exchanged one by one back and forth between to two parts of the chain (for a chain of 30 monomers). So the distribution of the span in the direction of the flow shows discrete peaks spaced out by a regular distance that corresponds to the size of one monomer.

This work could lead to numerous other studies. For example, the wall and solvent beads in our system interact with the chain monomers with the same potential. One could change the wall-chain interaction so the chain becomes either repelled by or attracted to the wall. The repulsive wall would push the chain into higher flow regions, while an attractive wall would do the opposite. In both cases, the regimes considered in this article may not be able to explain the new dynamics of the chain.

More simply, MD simulations could also be used to verify Buguin and Brochard-Wyart theories [7] of collapsed tethered chains submitted to a constant velocity flow profile. Oddly, to the best of our knowledge, such simulations or experiments have never been carried out.

Of course, longer chains (i.e., larger N) coupled with the use of a bending potential between consecutive monomers in the chain (the WLC model) would enable us to represent DNA molecules in greater detail. The problem at the moment is the computationally intensive nature of such calculations. Both new added features would dramatically increase the total CPU cycles needed to compute all the interactions and displacements, especially for longer chains, which imply bigger systems. Since DNA molecules have a long Kuhn length (are much stiffer than FJCs), simulations of large systems which would contain theses chains will only become a reality when CPU speeds improve substantially.

6 Acknowledgements

This work was supported by a Discovery Grant of the Natural Sciences and Engineering Research Council of Canada (NSERC) to GWS. YG would like to thank the Fonds Nature et Technologies (Québec) and the University of Ottawa for scholarships. This work used the computing resources of the High Performance Computing Virtual Laboratory (HPCVL), the Multimedia Advanced Computing Infrastructure (MACI), the Shared Hierarchical Academic Research Computing Network (SHARCNET) and the Western Canada Research Grid (WestGrid). Finally, the authors would like to thank Martin Kenward for useful discussions.

References

1. P. S. Doyle, B. Ladoux, and J. L. Viovy *Phys. Rev. Lett.*, vol. 84, pp. 4769–4772, 2000.
2. A. Ashkin, J. M. Dziedzic, J. E. Bjorkholm, and S. Chu *Optics Letters*, vol. 11, pp. 288–290, 1986.
3. T. T. Perkins, D. E. Smith, and S. Chu *Science*, vol. 264, pp. 819–822, 1994.
4. T. T. Perkins, S. R. Quake, D. E. Smith, and S. Chu *Science*, vol. 264, pp. 822–826, 1994.
5. F. Brochard-Wyart *Europhys. Lett.*, vol. 23, pp. 105–111, 1993.
6. F. Brochard-Wyart *Europhys. Lett.*, vol. 30, pp. 387–392, 1995.
7. A. Buguin and F. Brochard-Wyart *Macromolecules*, vol. 29, pp. 4937–4943, 1996.
8. B. Ladoux and P. S. Doyle *Europhys. Lett.*, vol. 52, pp. 511–517, 2000.
9. M. Rubinstein, *Polymer Physics*. Oxford University Press, 2003.
10. J. E. Mayer and M. G. Mayer, *Statistical Mechanics*. New York: J. Wiley & sons, 1940.
11. A. Rahman *Phys. Rev.*, vol. 136, pp. 405–411, 1964.
12. L. Verlet *Phys. Rev.*, vol. 159, pp. 98–103, 1967.
13. R. C. Armstrong *J. Chem. Phys.*, vol. 60, pp. 724–728, 1974.
14. G. S. Grest and K. Kremer *Phys. Rev. A*, vol. 33, pp. 3628–3631, 1986.
15. J. Koplik, J. R. Banavar, and J. F. Willemsen *Phys. Rev. Lett.*, vol. 60, pp. 1282–1285, 1988.
16. J. Gao and J. H. Weiner *Macromolecules*, vol. 29, pp. 6048–6055, 1996.
17. S. Barsky and G. W. Slater *Macromolecules*, vol. 32, pp. 6348–6358, 1999.
18. M. Kenward and G. W. Slater *European Physical Journal E*, vol. 14, pp. 55–65, 2004.
19. Y. Gratton and G. W. Slater submited to European Physical Journal E, 2005.

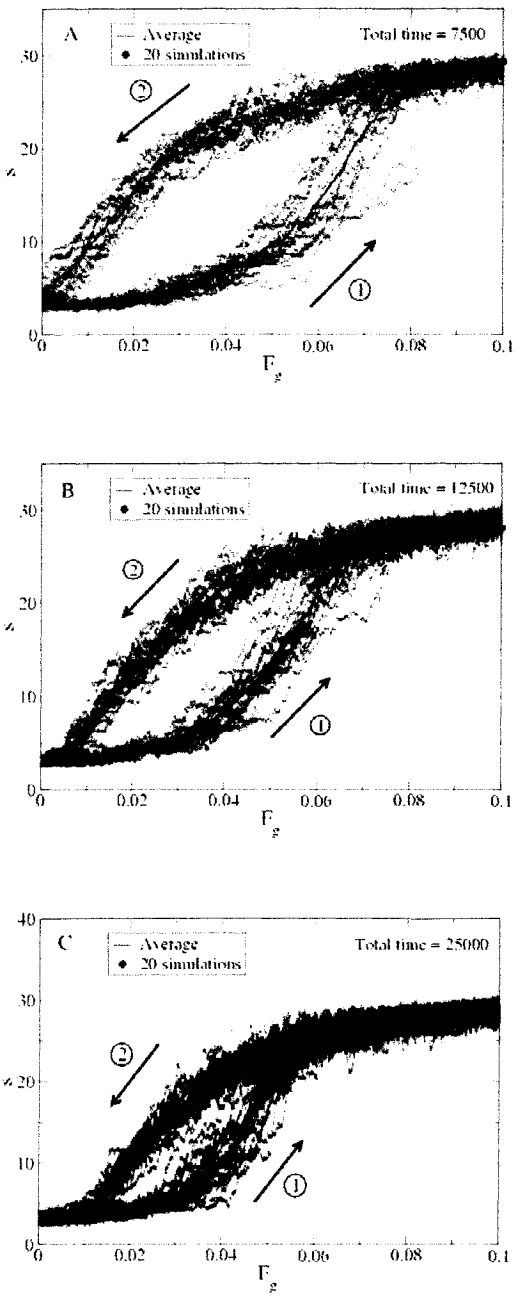

Fig. 9. *Average of 20 simulations per graph where the external force F_g varies from 0.0 to 0.1 then back to 0.0 in a different total amount of time t_T. The arrows show the direction of the movement. The presence of a hysteresis for s is quite evident in all cases. The total time t_T is 7500, 12500 and 25000 for A), B) and C) respectively.*

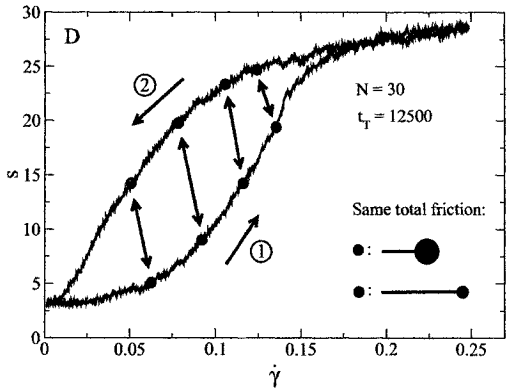

Fig. 10. *Example of the span trajectory with respect to $\dot{\gamma}$ while F_g is changed from 0.0 to 0.1 then back to 0.0. The pairs of dots (black with white) represent the spans and shear rates where both chain conformation experience the same friction force.*

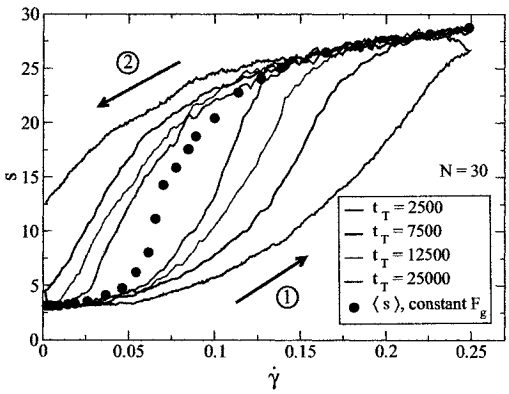

Fig. 11. *Combination of four different values of the ramping time t_T compared with the average span $\langle s \rangle$ when F_g is kept constant for the whole duration of the simulation.*

Conclusion

In this thesis, we studied simple but fundamental systems which involve a single chain tethered to a hard surface and submitted to a Poiseuille (shear) flow. The thesis is based on two manuscripts (see Chapters 2 and 3) and addresses two distinct situations: 1. the solvent is of good quality and 2. the solvent is of poor quality. Both manuscripts aim to provide a better understanding of the dynamics of a tethered Freely Jointed Chain (FJC) using Molecular Dynamics simulations and theoretical arguments.

Good solvent

Tethered polymers in good solvents exhibit rich dynamical behavior. Their range of extension in the direction of the flow can be separated into two distinct regimes: the weak stretching regime and the strong stretching regime. The models proposed by Ladoux and Doyle [7] (strong stretching regime) and by Brochard-Wyart [13] (weak stretching regime) agree with our simulation data. We also proposed a simple interpolation function which relates the unstretched fraction ε of the chain to the Weissenberg number Wi over the whole range of shear rates (weak and strong):

$$\varepsilon = \frac{1}{1 + \left(\frac{Wi}{Wi^*}\right)^{2/3}} \tag{4.1}$$

where the critical Weissenberg number Wi^* is an indication of the shear rate limit between these regimes. For $Wi \gg Wi^*$, equation (4.1) has the same scaling law as the strong stretching regime prediction of Ladoux and Doyle [7] ($\varepsilon \cong Wi^{-2/3}$). For $Wi \ll Wi^*$, equation (4.1) does not predict the theoretical scaling law proposed by Brochard-Wyart [13] for the weak stretching regime ($\varepsilon \cong 1 - Wi^{2/3}$ compared to $\varepsilon \cong 1 - Wi^{1/2}$), but it does agree with a simple Pincus blob theory. Even though the Brochard-Wyart weak stretching theory does not agree perfectly with our interpolation function, it provides a good fit of our MD data over a small section of Wi.

We extended our analysis of the problem by looking at the dependence of the critical Weissenberg number Wi^* on the number of monomers N in the chain. We found from a scaling analysis of the strong stretching limit that Wi^* scales like $N^{3/10}$. Using $Wi^* = Wi_0 N^{3/10}$ in our interpolation function, we determined that Wi_0 is consistent for $N = 20$, 30 and 40 at around 4.1. One would need to simulate much longer chains to verify the universality of equation (4.1) and Wi_0.

The chain end-to-end distance in the direction of the flow fluctuates significantly for small Wi. In this region, a four-step cyclic motion is observed in two ways. First, direct visualization shows that the

cyclic motion happens randomly. Second, a cross-correlation function between the end-to-end distance and the angle between the wall and the vector joining the anchor to the center of mass of the chain clearly demonstrates the presence of the cyclic motion. This motion disappears with increasing Wi. These particular dynamics of the chain are in agreement with the cyclic motion observed experimentally for DNA molecules in a good solvent in Ref. [5].

We found that the duration of the chain recirculation cycle τ_+ ($\sim NWi^{-2/3}$) coupled with equation (4.1) leads naturally to the following formula:

$$\varepsilon = \frac{1}{1 + \frac{\tau_0}{\tau_+}}, \tag{4.2}$$

where the critical time τ_0 scales like $N^{4/5}$. Furthermore, we determined that the nonequilibrium relaxation time of a stretched chain also scales like $N^{4/5}$. Therefore, the critical time τ_0 must be the nonequilibrium relaxation time, and thus equation (4.2) defines the competition between the shear forces (i.e., τ_+) and the entropic relaxation (i.e., τ_0) of a stretched polymer chain.

The explicit solvent particles in our MD simulations allowed us to observe the effects of hydrodynamic interactions. For instance, we were able to determine that the flow profile created from a constant external force is a Poiseuille flow. Also, the solvent near the walls follows a no-slip boundary condition. More importantly, we observed a self-consistent interaction between the chain and the solvent. The shear flow does affect the chain conformations, but the converse, which is often overlooked in theories, also occurs: the chain affects the flow. In one of our simulations, a single chain was able to modified the local shear rate by up to 18% compared to its value in the absence of the chain.

In this thesis, the system size used in our MD simulations would not accurately describe macroscopic systems, but rather nanoscopic ones. For this reason some reported effects are not likely to be observed in macroscopic systems. For example, we showed that the free end of the chain prefers distinct positions along the wall compared to others, which relates to the layering of the solvent particles close to the wall. This effect is in part an artifact arising from the structure of the wall itself: the wall is perfectly flat with beads spaced out evenly in a lattice structure. Another effect that should only be seen in the nanoscopic regime is the sticking of the chain to the wall. For times comparable to the equilibrium relaxation time of the chain, the polymer stays in a stretched conformation while sticking to the wall. Since no attractive potential is used for the wall-polymer interactions, the answer lies in entropic and packing effects.

Poor solvent

A polymer chain surrounded by poor solvent will collapse onto itself since its own monomers prefer to be close to each other. This collapsed conformation entirely changes the scaling laws for the extension versus the shear rate. We simplified the Buguin and Brochard-Wyart [16] theory of the stretching of collapsed chains to three regimes: the *small deformation* regime where the chain stays in a globule conformation, the *stem and globule* regime where the globule is attached to the tethering point by a stem (linear string of monomers), and the *ideal chain* regime where the strong flow completely extends the chain to its maximum extension. We found that all three regimes agree nicely with our MD simulation data for chain lengths N of 20, 30 and 40 beads.

As in the good solvent case, large fluctuations of the chain extension along the direction of the flow for shear rates in the *stem and globule* regime were an indication of new dynamical properties. A detailed study of the fluctuations revealed that the chain span preferred discrete values spaced out evenly by intervals of the size of one monomer. We attribute these evenly spaced peaks in the probability distribution function to a competition between the globule and the stem to add monomers of the other part to its own. On the other hand, no cyclic motion was observed either visually or with the extension-angle cross-correlation functions. The reason lies in the conformation taken by the chain in the *stem and globule* regime. Since the top of the globule experiences stronger flows, the globule is always pushed down against the wall like a lever. One of the conditions to get a cyclic motion in this type of system is that the chain has to leave the proximity of the wall and explore stronger flows (which will extend it and continue the cycle). Since this initial condition never occurs, the cyclic motion is prevented.

A special scenario where the shear rate changes linearly in time from zero to a maximum value then back to zero was also studied. We observed a large rate-dependent hysteresis in the force extension curve. We explained that this property comes from the difference between the friction coefficient of a globule and of a rod aligned in the direction of the flow. We presented an approximate calculation to determine at which two shear rates the chain can feel the same total friction force. Also, it is clear that if two possible chain conformations can co-exist at a given shear rate, the longer one will eventually collapse to the small chain span via thermal fluctuations.

Ideas for future projects

One simple modification to the simulation program would be to include bending potentials between consecutive monomers in the chain (which would now be considered as a WLC). One application would

be to investigate the dynamics of tethered DNA molecules (which behave like WLCs) in good and poor solvents. Longer chains would need to be used to represent DNA molecules, which creates a "temporary" problem: longer chains imply bigger systems, which in turn imply an increased number of interactions to calculate per simulation, hence additional months or years of CPU time. This type of project should be accessible in the years to come when computer speeds increase enough to finish MD simulations of larger systems in practical time.

With both types of solvent, one could include an attraction or repulsion for polymer-wall interactions. The repulsion scenario would cause the chain to explore stronger flows far away from the wall. For good and poor solvents, the chain should extend at a faster rate compared to the case where there is no added repulsion. On the other hand, the cyclic motions observed for good solvents would be in question: since the chain is not likely to approach the wall, and preferably remain in strong flows, the relaxation step of the cycle near the wall would be more difficult.

An attraction between the chain and the wall, on the other hand, would completely change this picture. Since the chain would prefer then to lie near the wall, it would take quite a strong shear flow to stretch the chain. Again the cyclic motion would be compromised since the first step of the cycle (leaving the proximity of the wall to explore stronger flows) would occur rarely.

Another direction an eventual project could take is to study in detail what happens if the solvent property suddenly changes from good to poor or vice versa. Certainly the chain would collapse in the first case, while it would swell in the second case, but the dynamics of these swelling/collapsing processes are unknown. The conditions to get a solvent where the chain is in an ideal conformation could be found, which an analysis of the chain conformations could verify. In this thesis, we made the well of the Lennard-Jones potential deeper for polymer-polymer interactions to collapse the chain. Another possibility exists which would have the same effect: the temperature of the system can provoke the collapse or swelling of chains. A study on the effect of temperature on tethered chains could be another possibility for future work.

A new application that would include both studies of this thesis would be the conception of a polymer valve in a nanocapillary. In past studies [3], it has been shown that walls coated with polymer brushes could act as a valve in a tube: when good solvent was flowed inside the tube, the polymer chains swell and stop the flow, but when poor solvent comes in contact with the chains, they collapse and let the flow pass. The new idea would work only in nanocapillaries. Let's consider a system which include two polymer chains tethered (opposite to each other) by one end to the wall of a nanochannel (see Fig. 4.1). The chain lengths must be chosen in a way that when the chains collapse under poor

solvent conditions, the globule radius is close to the channel radius. This condition would make the chains block the capillary completely when poor solvents come in contact with them. With properly chosen good solvents, the chains would swell and wet the walls, letting the flow of solvent pass in the capillary.

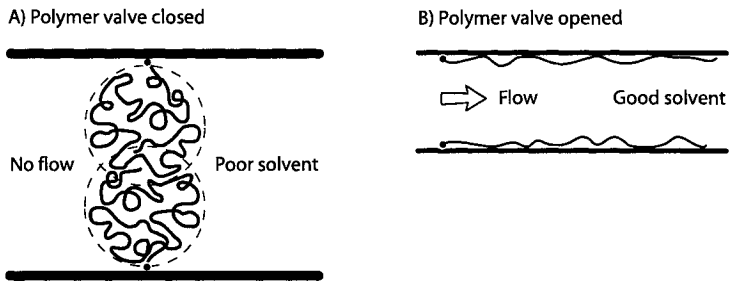

Figure 4.1: *Schematic example of the polymer valve. A) The chains block the solvent flow under a poor solvent case. B) A good solvent coupled with an polymer-wall attraction unblocks the capillary.*

The key is the attractive potential between the wall and the chains. The polymer-wall potential would attract the chains towards the wall, which would allow the flow to move more freely in the middle of the capillary since the chains would be out of the way. One problem that could arise with the addition of the attractive potential is that if the potential is too strong compared to the polymer-polymer potential, the chains would never collapse and the polymer valve would not work. A good choice for the strength of the polymer-wall interaction is thus critical for this application to work. Such a system could be easily studied via MD simulations, of course, but experimental work on this problem could pose quite a challenge.

Bibliography

[1] A. P. Doig Jr. *Genetic Engineering News*, 25:26–27, 2005.

[2] G. W. Slater, S. Guillouzic, M. G. Gauthier, J. F. Mercier, M. Kenward, L. C. McCormick, and F. Tessier. *Electrophoresis*, 23:3791–3816, 2002.

[3] E. M. Sevick and D. R. M. Williams. *Macromolecules*, 27:5285–5290, 1994.

[4] J. Klein, Y. Kamiyama, H. Yoshizawa, J. N. Israelachvili, G. H. Fredrickson, P. Pincus, and L. J. Fetters. *Macromolecules*, 26:5552–5560, 1993.

[5] P. S. Doyle, B. Ladoux, and J. L. Viovy. *Phys. Rev. Lett.*, 84:4769–4772, 2000.

[6] J. L. Harden, D. Long, and A. Ajdari. *Langmuir*, 17:705–715, 2001.

[7] B. Ladoux and P. S. Doyle. *Europhys. Lett.*, 52:511–517, 2000.

[8] M. Rubinstein and R. H. Colby. *Polymer Physics.* Oxford University Press, 2003.

[9] I. Teraoka. *Polymer Solutions: An Introduction to Physical Properties.* John Wiley & Sons, New York, 2002.

[10] P. G. deGennes. *Scaling Concepts in Polymer Physics.* Cornell University Press, 1979.

[11] G. W. Slater, Y. Gratton, M. Kenward, L. McCormick, and F. Tessier. *Soft Materials*, 1:365–391, 2003.

[12] P. Pincus. *Macromolecules*, 9:386–388, 1976.

[13] F. Brochard-Wyart. *Europhys. Lett.*, 23:105–111, 1993.

[14] F. Brochard-Wyart. *Europhys. Lett.*, 30:387–392, 1995.

[15] R. G. Larson T. T. Perkins, D. E. Douglas and S. Chu. *Science*, 268:83–87, 1995.

[16] A. Buguin and F. Brochard-Wyart. *Macromolecules*, 29:4937–4943, 1996.

[17] J. W. Hatfield and S. R. Quake. *Phys. Rev. Lett.*, 82:3548–3551, 1999.

[18] J. F. Marko and E. D. Siggia. *Macromolecules*, 28:8759–8770, 1995.